Numer. Math. Theor. Meth. Appl.
doi: 10.4208/nmtma.OA-2021-0184

Vol. **16**, No. 1, pp. 242-276
February 2023

The Direct Method of Lines for Forward and Inverse Linear Elasticity Problems of Composite Materials in Star-shaped Domains

Xiaopeng Zhu[1], Zhizhang Wu[2,*] and Zhongyi Huang[1]

[1] *Department of Mathematical Sciences, Tsinghua University, Beijing 100084, China*
[2] *Department of Mathematics, The University of Hong Kong, Pokfulam Road, Hong Kong SAR, China*

Received 3 December 2021; Accepted (in revised version) 10 July 2022

Abstract. In this paper, we generalize the direct method of lines for linear elasticity problems of composite materials in star-shaped domains and consider its application to inverse elasticity problems. We assume that the boundary of the star-shaped domain can be described by an explicit C^1 parametric curve in the polar coordinate. We introduce the curvilinear coordinate, in which the irregular star-shaped domain is converted to a regular semi-infinite strip. The equations of linear elasticity are discretized with respect to the angular variable and we solve the resulting semi-discrete approximation analytically using a direct method. The eigenvalues of the semi-discrete approximation converge quickly to the true eigenvalues of the elliptic operator, which helps capture the singularities naturally. Moreover, an optimal error estimate of our method is given. For the inverse elasticity problems, we determine the Lamé coefficients from measurement data by minimizing a regularized energy functional. We apply the direct method of lines as the forward solver in order to cope with the irregularity of the domain and possible singularities in the forward solutions. Several numerical examples are presented to show the effectiveness and accuracy of our method for both forward and inverse elasticity problems of composite materials.

AMS subject classifications: 65N21, 65N40, 74A40, 74B05
Key words: Composite materials, linear elasticity problems, inverse elasticity problems, star-shaped domains, method of lines.

1. Introduction

With the growing application of composite materials, the linear elasticity problem

*Corresponding author. *Email addresses:* zxp17@mails.tsinghua.edu.cn (X. Zhu), wuzz@hku.hk (Z. Wu), zhongyih@tsinghua.edu.cn (Z. Huang)

of composite materials has drawn a great deal of attention from mathematicians and engineers. In this paper, we focus on both forward and inverse linear elasticity problems of composite materials in star-shaped domains. We first describe and make some assumptions on the geometry of the star-shaped domain $\overline{\Omega} = \bigcup_{k=1}^{K} \overline{\Omega}_k \subset \mathbb{R}^2$, where Ω stands for the whole material composed of K kinds of different materials and Ω_k stands for the k-th kind of material. We assume that the boundary $\Gamma = \partial\Omega$ is star-shaped with respect to the origin O and can be described by an explicit C^1 parametric curve in the polar coordinates. To be more precise, we assume that Γ can be parameterized as a (piecewise) C^1 function of the angular variable ϕ, denoted by $\tilde{r}(\phi)$, such that $\tilde{r}(0) = \tilde{r}(2\pi)$ and $\tilde{r}(\phi) \geq r_0 > 0$ for any $0 \leq \phi \leq 2\pi$. This assumption on the geometry of Γ is made so that the curvilinear coordinate which will be introduced in (2.1) is well defined; see also (2.3)-(2.11). Without loss of generality, we also assume that all the interfaces between different materials meet at the origin and each interface $\overline{\Omega}_{k-1} \cap \overline{\Omega}_k$ is a line segment

$$L_k = \big\{(r,\theta)\,|\,\theta = \theta_k,\, 0 \leq r \leq \tilde{r}(\theta_k)\big\} \quad \text{for} \quad k = 1, \ldots, K,$$

where $\Omega_0 = \Omega_K, \theta_1 = 0$ (See Fig. 1).

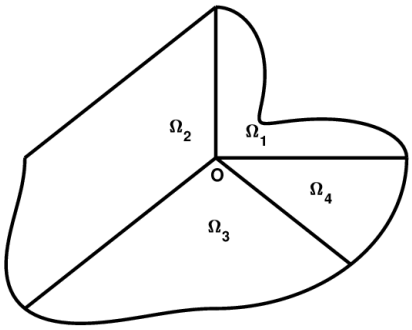

Figure 1: Composite materials in a star-shaped domain.

We also let $\theta_{K+1} = 2\pi$. We consider the following Navier's equations in Ω with Dirichlet boundary conditions, which describe the equilibrium state in linear elasticity:

$$\begin{aligned} -\nabla \cdot \sigma^k &= 0 && \text{in } \Omega_k, \\ u^k &= f^k && \text{on } \Gamma_k, \\ u^{k-1}|_{\theta=\theta_k^-} &= u^k|_{\theta=\theta_k^+}, \\ \sigma^{k-1} \cdot n_k|_{\theta=\theta_k^-} &= \sigma^k \cdot n_k|_{\theta=\theta_k^+} \end{aligned} \tag{1.1}$$

with

$$\sigma^k = 2\mu_k \varepsilon(u^k) + \lambda_k \nabla \cdot u^k I, \quad \varepsilon(u^k) = \frac{1}{2}\big(\nabla u^k + (\nabla u^k)^T\big), \tag{1.2}$$

where $k = 1, \ldots, K$, $\Gamma_k = \partial\Omega_k \bigcap \partial\Omega$, f is a given vector-valued function on Γ

$$f|_{\Gamma_k} = f^k = \big(f_1^k, f_2^k\big)^T,$$

u is the displacement in Ω and

$$u|_{\Omega_k} = u^k = \big(u_1^k, u_2^k\big)^T,$$

σ is the stress tensor in Ω and $\sigma|_{\Omega_k} = \sigma^k$, and

$$n_k = \big(-\sin(\theta_k), \cos(\theta_k)\big)^T.$$

μ and λ are the piecewise constant Lamé coefficients and take constant values $\mu_k > 0$, $\lambda_k > 0$ in Ω_k, respectively. The forward problem for (1.1) aims to compute the displacement u given the Lamé coefficients μ and λ, while the inverse problem for (1.1) aims at determining the Lamé coefficients μ and λ from a measurement of u.

For the forward problem, one major difficulty is the stress singularity, which may appear at the intersection of interfaces, edges and the crack tips. Many mathematicians have made their efforts to investigations on the singularities of composite materials in elliptic problems. Babuška [3,4] and Kellogg [31,32] studied the interface problem for elliptic equations, which is a model problem of composite materials. The structures of the stress singularities in dissimilar materials were discussed in [9,12,38,41,42,49,52], and it was found that the stress would admit oscillatory behaviours near the interfaces and crack tips. We know from [18,38,45] that the singular part of the local solution of (1.1) around the origin takes the form of

$$u^s = \big(u_1^s, u_2^s\big)^T = \sum_j a_j r^{b_j} \big(\Phi_j(\phi), \Psi_j(\phi)\big)^T$$

in the polar coordinate, where b_j are eigenvalues, Φ_j and Ψ_j are smooth eigenfunctions, and the coefficients a_j are called generalized stress intensity factors. In particular, $0 < \mathbf{Re}(b_j) < 1$ for all j, where $\mathbf{Re}(b_j)$ is the real part of b_j. Hence, singularities occur in the stress σ when $a_j \neq 0$ for some j. Furthermore, when $a_j \neq 0$ for some j, the displacement $u \in H^1(\Omega)$ but $u \notin H^2(\Omega)$, and thus a direct application of traditional methods like finite element methods (FEM) [2] and finite difference methods [7] to (1.1) would suffer from reduced convergence rates. To improve the numerical result, many different methods have been developed by mathematicians and engineers over the past few decades. To name a few, there are mesh refinements [5, 36], the infinite element method [23], the boundary element method [34, 40], the use of singular functions in FEM [13, 35], the finite strip method [10], the method of auxiliary mapping [37], the adaptive mixed FEM [8], the adaptive discontinuous Galerkin FEM [48], the corrected extended FEM [14], the stable generalized FEM [22] and the extended isogeometric analysis [15], etc. In general, more accurate numerical solutions can be obtained by the above-mentioned methods for given problems. However, there are still some limitations in each approach. For instance, several methods require a prior knowledge of the structure of the singularity at the singular point of a given problem, including the method of auxiliary mapping, the extended isogeometric analysis, etc.

Among all, the direct method of lines, a semi-discrete method which is a development of the method of lines [44, 51], has received much attention in solving singular elliptic problems. This method requires no prior information of the singularities

and is able to construct an accurate solution. The direct method of lines was introduced to deal with elliptic problems with singularities on a polygonal domain [26, 27] and boundary value problems on an unbounded domain [24, 25]. Recently, the direct method of lines was generalized in [50] for solving the Laplace's equation with singularities in star-shaped domains.

In this paper, our first goal is to generalize the direct method of lines for solving (1.1) in star-shaped domains. To handle the irregularity of the star-shaped domain, a curvilinear coordinate is introduced so that the star-shaped domain is converted to a regular semi-infinite strip. Then (1.1) is reduced to an equivalent variational-differential problem in the curvilinear coordinate. An ODE system is obtained by discretizing the variational-differential problem with respect to the angular variable. The ODE system can be solved analytically using a direct method so that a semi-discrete solution can be constructed. It is numerically found that the eigenvalues of the ODE system converge quickly to the true eigenvalues of the elliptic operator and hence the singularities can be captured naturally by our method; see Section 5.1. Moreover, an optimal error estimate of our semi-discrete method can be given.

On the other hand, we consider the numerical solutions of the inverse elasticity problem, which is of significant importance as well. It has a successful application in the elasticity imaging (or elastography) for medical diagnosis [11, 21]. Moreover, the inverse elasticity problem also has an important application in the material characterization, which aims to identify the mechanical properties of materials, and such characterizations become more difficult in the case of composite materials; see e.g. [1, 19, 43] and the references therein. For the inverse elasticity problem in this work, we are still interested in the case of composite materials in a star-shaped domain as in the forward problem, where each interface between different materials is a line segment connecting the origin and a point on the boundary. Since full-field measurements can be obtained by various techniques [19, 20, 39], we assume here that the measurement of the displacement u in the entire domain is available. The second goal of this paper is to propose a numerical procedure for identifying the locations of the interfaces and recovering the values of Lamé coefficients on each subdomain from the measurement of u. Different computational frameworks have been proposed for solving this problem [1, 6, 16, 17, 28, 30]. We adopt the least-square approach [16]. The Lamé coefficients are approximated by piecewise constant functions. We estimate the Lamé coefficients by minimizing an energy functional in the least-square sense with total variation regularization [47] using the Adam algorithm [33], which is a gradient-based optimization algorithm. In each iteration, the forward problem is an interface problem in the star-shaped domain. To deal with the irregularity of the domain and possible singularities in the forward solutions, we adopt the direct method of lines as the forward solver. Numerical results show that our method is effective in reconstructing the Lamé coefficients.

The rest of the paper is organized as follows. In Section 2, we introduce the curvilinear coordinate and the semi-discrete approximation of the reduced variational-differential problem. Treatment to the linear elasticity problems with a traction and a body

force is given in Section 3. In Section 4, we propose a numerical procedure for solving the inverse elasticity problem with the direct method of lines as the forward solver. Several numerical examples of both forward and inverse elasticity problems are presented in Section 5. Finally, we draw some conclusions in Section 6.

2. The generalized direct method of lines for linear elasticity problems

2.1. The curvilinear coordinate

The star-shaped domain is generally irregular, which makes it hard to solve (1.1) on a regular stencil using traditional methods. Therefore, we introduce the curvilinear coordinate

$$(x,y)=e^{\rho}\big(\tilde{r}(\phi)\cos(\phi),\tilde{r}(\phi)\sin(\phi)\big),\quad 0\le\phi<2\pi,\quad -\infty<\rho\le 0. \tag{2.1}$$

The curvilinear coordinate (2.1) is well defined with the assumption on the geometry of Γ described in Section 1; see also (2.3)-(2.11). By the transformation of coordinates (2.1), we can map each subdomain Ω_k into a regular semi-infinite strip (See Fig. 2).

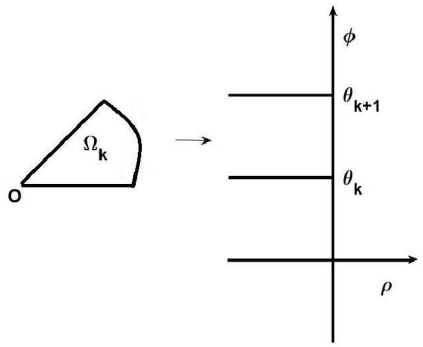

Figure 2: Transformation of coordinates by the curvilinear coordinate.

In this way, we can cope with more general irregular star-shaped domains. To derive the equivalent form of (1.1) in the curvilinear coordinate, we note that $\nabla=(\partial/\partial x,\partial/\partial y)^T$ and we have from (1.1)

$$\nabla\cdot\sigma^k=\mu_k\Delta u^k+(\lambda_k+\mu_k)\nabla(\nabla\cdot u^k),\quad k=1,\dots,K. \tag{2.2}$$

Then we introduce $D_c=(\partial/\partial\rho,\partial/\partial\phi)^T$ and set $E=(e_1,e_2)^T$, where

$$e_1=\partial_\rho\big(x(\rho,\phi),y(\rho,\phi)\big),$$
$$e_2=\partial_\phi\big(x(\rho,\phi),y(\rho,\phi)\big).$$

By the chain rule, we obtain

$$\nabla=E^{-1}D_c, \tag{2.3}$$

$$\nabla\cdot u^k=\left(\partial_\rho+2,\partial_\phi+2\frac{\tilde{r}'}{\tilde{r}}\right)E^{-T}u^k. \tag{2.4}$$

Hence, we have

$$\nabla(\nabla\cdot u^k)=E^{-1}D_c\left(\partial_\rho+2,\partial_\phi+2\frac{\tilde r'}{\tilde r}\right)E^{-T}u^k, \tag{2.5}$$

$$\Delta u_j^k=\nabla\cdot\left(\nabla u_j^k\right)=\left(\partial_\rho+2,\partial_\phi+2\frac{\tilde r'}{\tilde r}\right)E^{-T}E^{-1}D_c u_j^k,\quad j=1,2. \tag{2.6}$$

Combining (2.2), (2.5) and (2.6), we have in the curvilinear coordinate

$$e^{2\rho}\tilde r(\phi)^2\nabla\cdot\sigma^k=\left(Q_1^k,Q_2^k\right)^T, \tag{2.7}$$

where

$$\begin{aligned}Q_j^k=&\partial_\rho\left(t_{j,1}^k\partial_\rho u_1^k+t_{j,2}^k\partial_\phi u_1^k+t_{j,3}^k\partial_\rho u_2^k+t_{j,4}^k\partial_\phi u_2^k\right)\\&+\partial_\phi\left(t_{j,5}^k\partial_\rho u_1^k+t_{j,6}^k\partial_\phi u_1^k+t_{j,7}^k\partial_\rho u_2^k+t_{j,8}^k\partial_\phi u_2^k\right)\end{aligned} \tag{2.8}$$

for $j=1,2$ with

$$\begin{aligned}
t_{1,1}^k&=\left(1+\left(\frac{\tilde r'}{\tilde r}\right)^2\right)\mu_k+(\lambda_k+\mu_k)\left(\frac{\tilde r'\sin(\phi)+\tilde r\cos(\phi)}{\tilde r}\right)^2,\\
t_{1,2}^k&=-(\lambda_k+\mu_k)\frac{\sin(\phi)\left(\tilde r'\sin(\phi)+\tilde r\cos(\phi)\right)}{\tilde r}-\mu_k\frac{\tilde r'}{\tilde r},\\
t_{1,3}^k&=-(\lambda_k+\mu_k)\frac{\left(\tilde r'\sin(\phi)+\tilde r\cos(\phi)\right)\left(\tilde r'\cos(\phi)-\tilde r\sin(\phi)\right)}{\tilde r^2},\\
t_{1,4}^k&=\mu_k\frac{\cos(\phi)\left(\tilde r'\sin(\phi)+\tilde r\cos(\phi)\right)}{\tilde r}+\lambda_k\frac{\sin(\phi)\left(\tilde r'\cos(\phi)-\tilde r\sin(\phi)\right)}{\tilde r},\\
t_{1,5}^k&=t_{1,2}^k,\quad t_{1,6}^k=\mu_k+\sin^2(\phi)(\lambda_k+\mu_k),\\
t_{1,7}^k&=\lambda_k\frac{\cos(\phi)\left(\tilde r'\sin(\phi)+\tilde r\cos(\phi)\right)}{\tilde r}+\mu_k\frac{\sin(\phi)\left(\tilde r'\cos(\phi)-\tilde r\sin(\phi)\right)}{\tilde r},\\
t_{1,8}^k&=-(\lambda_k+\mu_k)\cos(\phi)\sin(\phi),\quad t_{2,1}^k=t_{1,3}^k,\quad t_{2,2}^k=t_{1,7}^k,\\
t_{2,3}^k&=\left(1+\left(\frac{\tilde r'}{\tilde r}\right)^2\right)\mu_k+(\lambda_k+\mu_k)\left(\frac{\tilde r'\cos(\phi)-\tilde r\sin(\phi)}{\tilde r}\right)^2,\\
t_{2,4}^k&=-(\lambda_k+\mu_k)\frac{\cos(\phi)\left(\tilde r'\cos(\phi)-\tilde r\sin(\phi)\right)}{\tilde r}-\mu_k\frac{\tilde r'}{\tilde r},\\
t_{2,5}^k&=t_{1,4}^k,\quad t_{2,6}^k=t_{1,8}^k,\quad t_{2,7}^k=t_{2,4}^k,\quad t_{2,8}^k=\mu_k+\cos^2(\phi)(\lambda_k+\mu_k).
\end{aligned} \tag{2.9}$$

On the other hand, by combining (1.2), (2.3) and (2.4), the stress tensor in the curvilinear coordinate is expressed as

$$\sigma^k=\begin{pmatrix}\sigma_{11}^k&\sigma_{12}^k\\\sigma_{21}^k&\sigma_{22}^k\end{pmatrix}, \tag{2.10}$$

where

$$\begin{aligned}
\sigma_{11}^k &= \frac{1}{e^{\rho}\tilde{r}^2}\Big((\lambda_k+2\mu_k)\big(\tilde{r}'\sin(\phi)+\tilde{r}\cos(\phi)\big)\partial_\rho u_1^k-(\lambda_k+2\mu_k)\tilde{r}\sin(\phi)\partial_\phi u_1^k\\
&\qquad -\lambda_k\big(\tilde{r}'\cos(\phi)-\tilde{r}\sin(\phi)\big)\partial_\rho u_2^k+\lambda_k\tilde{r}\cos(\phi)\partial_\phi u_2^k\Big),\\
\sigma_{12}^k &= \sigma_{21}^k=\frac{\mu_k}{e^{\rho}\tilde{r}^2}\Big(\big(\tilde{r}'\sin(\phi)+\tilde{r}\cos(\phi)\big)\partial_\rho u_2^k-\tilde{r}\sin(\phi)\partial_\phi u_2^k\\
&\qquad -\big(\tilde{r}'\cos(\phi)-\tilde{r}\sin(\phi)\big)\partial_\rho u_1^k+\tilde{r}\cos(\phi)\partial_\phi u_1^k\Big),\\
\sigma_{22}^k &= \frac{1}{e^{\rho}\tilde{r}^2}\Big(-(\lambda_k+2\mu_k)\big(\tilde{r}'\cos(\phi)-\tilde{r}\sin(\phi)\big)\partial_\rho u_2^k+(\lambda_k+2\mu_k)\tilde{r}\cos(\phi)\partial_\phi u_2^k\\
&\qquad +\lambda_k\big(\tilde{r}'\sin(\phi)+\tilde{r}\cos(\phi)\big)\partial_\rho u_1^k-\lambda_k\tilde{r}\sin(\phi)\partial_\phi u_1^k\Big).
\end{aligned}\tag{2.11}$$

We also have $dxdy=e^{2\rho}\tilde{r}(\phi)^2d\rho d\phi$ by the change of variables. Therefore, in the curvilinear coordinate, (1.1) is converted to

$$\begin{aligned}
&\big(Q_1^k,Q_2^k\big)^T=0,\quad \theta_{k-1}<\phi<\theta_k,\quad -\infty<\rho<0,\\
&u^k|_{\rho=0}=f^k(\phi),\quad \theta_{k-1}<\phi<\theta_k,\\
&u^{k-1}\big(\rho,\theta_k^-\big)=u^k\big(\rho,\theta_k^+\big),\\
&\begin{pmatrix}\sigma_{11}^{k-1}\sin(\theta_k)-\sigma_{12}^{k-1}\cos(\theta_k)\\ \sigma_{21}^{k-1}\sin(\theta_k)-\sigma_{22}^{k-1}\cos(\theta_k)\end{pmatrix}\Big|_{\theta=\theta_k^-}=\begin{pmatrix}\sigma_{11}^{k}\sin(\theta_k)-\sigma_{12}^{k}\cos(\theta_k)\\ \sigma_{21}^{k}\sin(\theta_k)-\sigma_{22}^{k}\cos(\theta_k)\end{pmatrix}\Big|_{\theta=\theta_k^+},
\end{aligned}\tag{2.12}$$

where $k=1,\dots,K$ and u^k is bounded when $\rho\to-\infty$. Let

$$\begin{aligned}
&H_p^1\big((0,2\pi)\big)=\Big\{v(\phi)|\, v(\phi),\, v'(\phi)\in L^2\big((0,2\pi)\big),\, v(0)=v(2\pi)\Big\},\\
&W=H_p^1\big((0,2\pi)\big)\times H_p^1\big((0,2\pi)\big),\\
&V=\Big\{v=\big(v_1(\rho,\phi),v_2(\rho,\phi)\big)^T\big|\, v,\partial_\rho v,\partial_{\rho\rho}^2 v\in W\ \text{ for any fixed }\ \rho<0\Big\}.
\end{aligned}$$

Then (2.12) is equivalent to the following variational-differential problem: Find $u(\rho,\phi)\in V$ such that

$$\begin{aligned}
&\frac{d^2A_2(u,v)}{d\rho^2}+\frac{dA_1(u,v)}{d\rho}+A_0(u,v)=0,\quad \forall v\in W,\quad -\infty<\rho<0,\\
&u|_{\rho=0}=f,
\end{aligned}\tag{2.13}$$

where u is bounded when $\rho\to-\infty$ and

$$A_2(u,v)=\sum_{k=1}^K\int_{\theta_k}^{\theta_{k+1}}u^k(\rho,\phi)^T\Psi_2^kv^k(\phi)d\phi,\tag{2.14}$$

$$A_1(u,v)=\sum_{k=1}^K\int_{\theta_k}^{\theta_{k+1}}\left(\left(\frac{\partial u^k(\rho,\phi)}{\partial\phi}\right)^T\Psi_1^kv^k(\phi)-u^k(\rho,\phi)^T\big(\Psi_1^k\big)^T\frac{dv^k(\phi)}{d\phi}\right)d\phi,\tag{2.15}$$

$$A_0(u,v) = -\sum_{k=1}^{K} \int_{\theta_k}^{\theta_{k+1}} \left(\frac{\partial u^k(\rho,\phi)}{\partial \phi}\right)^T \Psi_0^k \frac{dv^k(\phi)}{d\phi} d\phi \tag{2.16}$$

with $v^k = v|_{[\theta_k,\theta_{k+1}]}$ and

$$\Psi_2^k = \begin{pmatrix} t_{1,1}^k & t_{1,3}^k \\ t_{1,3}^k & t_{2,3}^k \end{pmatrix}, \quad \Psi_1^k = \begin{pmatrix} t_{1,2}^k & t_{1,4}^k \\ t_{1,7}^k & t_{2,4}^k \end{pmatrix}, \quad \Psi_0^k = \begin{pmatrix} t_{1,6}^k & t_{1,8}^k \\ t_{1,8}^k & t_{2,8}^k \end{pmatrix}. \tag{2.17}$$

It is easy to obtain the following lemma.

Lemma 2.1. *The following statements hold true:*

(1) $A_j(u,v),\ j=0,1,2$ *are bounded bilinear forms on* $W \times W$.

(2) A_0, A_2 *are symmetric,* A_1 *is antisymmetric on* $W \times W$.

(3) Let $\|\cdot\|_2$ *be the* L^2 *norm. There exists a constant* $c > 0$ *such that*

$$-A_0(v,v) \geq c\|v'\|_2^2, \quad A_2(v,v) \geq c\|v\|_2^2, \quad \forall v \in W.$$

2.2. The semi-discrete approximation of the variational-differential problem

We introduce the numerical solution of (2.13). Let

$$0 = \phi_1 < \cdots < \phi_{M+1} = 2\pi$$

be a partition of $[0, 2\pi]$, such that each of $\{\theta_k\}_{k=1}^K$ is a node of this partition, i.e. for each θ_k, there is a $\phi_j = \theta_k$. Let

$$h = \max_{1 \leq j \leq M} |\phi_{j+1} - \phi_j|$$

and W_1^h be any finite-dimensional subspace of $H_p^1((0,2\pi))$. We further let

$$W^h = W_1^h \times W_1^h,$$
$$V^h = \left\{ v = \big(v_1(\rho,\phi), v_2(\rho,\phi)\big)^T \,\middle|\, v, \partial_\rho v, \partial_{\rho\rho}^2 v \in W^h \ \text{ for any fixed } \ \rho < 0 \right\}.$$

Then we can approximate (2.13) with the following semi-discrete approximation: Find $u^h(\rho,\phi) \in V^h$ such that

$$\begin{aligned} &\frac{d^2 A_2(u^h, v^h)}{d\rho^2} + \frac{dA_1(u^h, v^h)}{d\rho} + A_0(u^h, v^h) = 0, \quad \forall v^h \in W^h, \quad -\infty < \rho < 0, \\ &u^h|_{\rho=0} = f^h(\phi), \end{aligned} \tag{2.18}$$

where u^h is bounded when $\rho \to -\infty$, $f^h(\phi) \in W^h$ and $f^h(\phi_j) = f(\phi_j)$ for $j = 1, \ldots, M$. A usual choice for W_1^h is the finite element space. In the following discussion, we choose W_1^h to be the linear element subspace of $H_p^1((0, 2\pi))$, i.e.

$$W_1^h = \Big\{ v(\phi) \,\Big|\, v \in H_p^1\big((0,2\pi)\big) \bigcap C\big([0,2\pi]\big), \\ v|_{[\phi_j,\phi_{j+1}]} \in P_1\big([\phi_j, \phi_{j+1}]\big),\ j = 1, \ldots, M \Big\}. \tag{2.19}$$

Let $\{N_j(\phi)\}_{j=1}^M$ be the basis functions of W_1^h such that $N_j(\phi_k) = \delta_{kj}, 1 \le k, j \le M$ and

$$N(\phi) = \begin{pmatrix} N_1(\phi) & \ldots & N_M(\phi) & 0 & \ldots & 0 \\ 0 & \ldots & 0 & N_1(\phi) & \ldots & N_M(\phi) \end{pmatrix}^T.$$

For $u^h(\rho, \phi) \in V^h$, let

$$U(\rho) = \Big(u_1^h(\rho, \phi_1), \ldots, u_1^h(\rho, \phi_M), u_2^h(\rho, \phi_1), \ldots, u_2^h(\rho, \phi_M)\Big)^T.$$

Then

$$\begin{aligned} u^h(\rho, \phi) &= N^T(\phi) U(\rho), \\ f^h(\phi) &= N^T(\phi) F, \end{aligned} \tag{2.20}$$

where

$$F = \big(f_1(\phi_1), \ldots, f_1(\phi_M), f_2(\phi_1), \ldots, f_2(\phi_M)\big)^T.$$

Hence, (2.18) is equivalent to the following boundary value problem of a second-order ODE system:

$$\begin{aligned} &B_2 U''(\rho) + B_1 U'(\rho) + B_0 U(\rho) = 0, \quad -\infty < \rho < 0, \\ &U|_{\rho=0} = F, \end{aligned} \tag{2.21}$$

where U is bounded when $\rho \to -\infty$ and

$$B_2 = \sum_{k=1}^K \int_{\theta_k}^{\theta_{k+1}} N(\phi) \Psi_2^k N(\phi)^T d\phi, \tag{2.22}$$

$$B_1 = \sum_{k=1}^K \int_{\theta_k}^{\theta_{k+1}} \Big(N(\phi) \Psi_1^k N'(\phi)^T - N'(\phi) \big(\Psi_1^k\big)^T N(\phi)^T \Big)\, d\phi, \tag{2.23}$$

$$B_0 = -\sum_{k=1}^K \int_{\theta_k}^{\theta_{k+1}} N'(\phi) \Psi_0^k N'(\phi)^T d\phi. \tag{2.24}$$

$B_j, j = 0, 1, 2$ – three $2M \times 2M$ constant matrices. From Lemma 2.1, we have

Lemma 2.2. *B_2 is a symmetric positive definite matrix, B_1 is an antisymmetric matrix and B_0 is a semi-negative definite symmetric matrix.*

We now apply a direct method to solve (2.21). Let

$$U(\rho) = e^{\rho\gamma}\xi, \tag{2.25}$$

where γ is a constant and $\xi \in \mathbb{C}^{2M}$, both of which are to be determined. Substituting (2.25) into (2.21), we obtain the quadratic eigenvalue problem

$$\big[\gamma^2 B_2 + \gamma B_1 + B_0\big]\xi = 0. \tag{2.26}$$

Let $\zeta = \gamma\xi$ and then the quadratic eigenvalue problem (2.26) is equivalent to the following general eigenvalue problem:

$$\begin{pmatrix} 0 & I_{2M} \\ -B_0 & -B_1 \end{pmatrix}\begin{pmatrix} \xi \\ \zeta \end{pmatrix} = \gamma \begin{pmatrix} I_{2M} & 0 \\ 0 & B_2 \end{pmatrix}\begin{pmatrix} \xi \\ \zeta \end{pmatrix}, \tag{2.27}$$

where I_{2M} is the $2M \times 2M$ identity matrix. From Lemma 2.2 and the result in [46], we have

Lemma 2.3. *The general eigenvalue problem* (2.27) *yields 2M eigenvalues with non-negative real parts while the other 2M eigenvalues have non-positive real parts.*

After solving (2.27) numerically, we would obtain $2M$ eigenvalues $\{\gamma_j^h\}_{j=1}^{2M}$ with non-negative real parts and their corresponding eigenvectors $(\xi_j^T, \zeta_j^T)^T$, $j = 1, \ldots, 2M$, where we can check that there are at least two zero eigenvalues. In particular, we assume that $\gamma_1^h = \gamma_2^h = 0$. Moreover, we let $\{\gamma_j^h\}_{j=1}^{2m}$ be the real eigenvalues in the ascending order and $\{\gamma_j^h\}_{j=2m+1}^{2M}$ be the complex eigenvalues with nonzero imaginary parts such that $\gamma_{2j}^h = \overline{\gamma}_{2j-1}^h$, $m+1 \le j \le M$. Then we have

$$U(\rho) = \sum_{j=1}^{2m} \alpha_j e^{\rho\gamma_j^h}\xi_j + \sum_{j=1+m}^{M} \Big(\alpha_{2j-1}\mathbf{Re}\big(e^{\rho\gamma_{2j}^h}\xi_{2j}\big) + \alpha_{2j}\mathbf{Im}\big(e^{\rho\gamma_{2j}^h}\xi_{2j}\big)\Big) \tag{2.28}$$

satisfying (2.21). By $U(0) = F$, we have

$$F = \sum_{j=1}^{2m} \alpha_j\xi_j + \sum_{j=1+m}^{M} \big(\alpha_{2j-1}\mathbf{Re}(\xi_{2j}) + \alpha_{2j}\mathbf{Im}(\xi_{2j})\big). \tag{2.29}$$

Denote

$$\begin{aligned} S(\rho) = \big[&e^{\rho\gamma_1^h}\xi_1, \ldots, e^{\rho\gamma_{2m}^h}\xi_{2m}, \mathbf{Re}(e^{\rho\gamma_{2m+2}^h}\xi_{2m+2}), \mathbf{Im}(e^{\rho\gamma_{2m+2}}\xi_{2m+2}), \ldots, \\ &\mathbf{Re}(e^{\rho\gamma_{2M}^h}\xi_{2M}), \mathbf{Im}(e^{\rho\gamma_{2M}^h}\xi_{2M})\big], \\ S(0) = \big[&\xi_1, \ldots, \xi_{2m}, \mathbf{Re}(\xi_{2m+2}), \mathbf{Im}(\xi_{2m+2}), \ldots, \mathbf{Re}(\xi_{2M}), \mathbf{Im}(\xi_{2M})\big], \\ \alpha = &[\alpha_1, \alpha_2, \ldots, \alpha_{2M}]^T. \end{aligned}$$

From (2.29), we have

$$\alpha = S(0)^{-1}F. \tag{2.30}$$

Substituting (2.30) into (2.28), we obtain

$$U(\rho) = S(\rho)S(0)^{-1}F \tag{2.31}$$

as the solution of (2.21). By (2.20), we obtain the semi-discrete solution of (2.13),

$$u^h(\rho,\phi) = N(\phi)^T S(\rho)S(0)^{-1}F. \tag{2.32}$$

To intuitively show how our method captures the singularities, we assume for simplicity that all the eigenvalues $\{\gamma_j^h\}_{j=1}^{2M}$ of the quadratic eigenvalue problem (2.26) are real, and the arguments are similar for the case where there exist complex eigenvalues. We can see from (2.32) that our method constructs the numerical solution in the form of

$$u^h = \sum_{j=1}^{2M} \alpha_j r^{\gamma_j^h} \big(\Phi_j^h(\phi), \Psi_j^h(\phi)\big)^T$$

in the polar coordinate, where

$$\Phi_j^h(\phi) = \big(\tilde{r}(\phi)\big)^{-\gamma_j^h} \sum_{k=1}^{M} N_k(\phi)(\xi_j)_k,$$
$$\Psi_j^h(\phi) = \big(\tilde{r}(\phi)\big)^{-\gamma_j^h} \sum_{k=1}^{M} N_k(\phi)(\xi_j)_{M+k}$$

with $(\xi_j)_k$ as the k-th component of ξ_j. It is numerically found that γ_j^h converges quickly to the true eigenvalue b_j of the elliptic operator and thus our method can naturally capture the singularities; see Section 5.1. Assume that u is the solution of (1.1) and we have the following error estimate, the proof of which is similar to that of in [27, Theorem 4.1].

Theorem 2.1. *If the linear elements are used, i.e. W_1^h is chosen to be* (2.19)*, there exists a positive constant C independent of h such that*

$$\|u - u^h\|_*^2 \le Ch^2 \sum_{j=1}^{2} \iint_\Omega \left(|\nabla u_j|^2 + \sum_{|\beta|=2} (x^2+y^2)|D^\beta u_j|^2 \right) dxdy, \tag{2.33}$$

where

$$\beta = (\beta_1,\beta_2)^T \in \mathbb{N}^2, \quad |\beta| = \beta_1+\beta_2, \quad D^\beta u_j = \frac{\partial^{|\beta|} u_j}{\partial x^{\beta_1}\partial y^{\beta_2}} \quad \textit{for} \quad j=1,2,$$

and for any $w, v \in H^1(\Omega)\times H^1(\Omega)$,

$$\|w\|_* = E(w,w)^{\frac{1}{2}} + |\psi_1(w)| + |\psi_2(w)| + |\psi_3(w)|,$$
$$\psi_1(w) = \int_\Gamma w_1 ds, \quad \psi_2(w) = \int_\Gamma w_2 ds, \quad \psi_3(w) = \int_\Gamma (w_1 y - w_2 x) ds,$$

$$E(w,v)=\sum_{k=1}^{K}\iint_{\Omega_k}\Big(\lambda_k(\nabla\cdot w^k)\cdot(\nabla\cdot v^k)+2\mu_k\big(\partial_x w_1^k\partial_x v_1^k+\partial_y w_2^k\partial_y v_2^k\big)$$
$$+\mu_k\big(\partial_y w_1^k+\partial_x w_2^k\big)\big(\partial_y v_1^k+\partial_x v_2^k\big)\Big)dx\,dy.$$

Recall that when $a_j\neq 0$ for some $j, u\in H^1(\Omega)$ but $u\notin H^2(\Omega)$, and thus $|\nabla u|^2$ is integrable but $|D^\beta u|^2$ is not integrable for $|\beta|=2$. Nevertheless, $r^2|D^\beta u|^2$ is integrable for $|\beta|=2$ since u admits singularities around the origin only in the r-direction in the polar coordinate in the form of $\mathcal{O}(r^{b_j})$ with $0<\mathbf{Re}(b_j)<1$ and is smooth with respect to ϕ. Thus in Theorem 2.1, the integral on the right-hand side of (2.33) is finite. Therefore, Theorem 2.1 shows that we can obtain the optimal first-order convergence for u in the energy norm $\|\cdot\|_*$ with linear elements used for semi-discretization, even if $u\notin H^2(\Omega)$. In addition, recalling that we assume $\lambda_k>0$ and $\mu_k>0$ for each k, we can see that

$$\|\sigma-\sigma^h\|_{L^2}\leq C\|u-u^h\|_*,$$

where σ is the stress tensor of (1.1), σ^h is the numerical stress tensor associated with u^h, and C is a constant independent of h. Therefore, Theorem 2.1 also shows that we can obtain the first-order convergence for a singular stress σ in the L^2 norm with linear elements used for semi-discretization if $\lambda>0$ and $\mu>0$. In practice, quadratic elements and other high-order elements can also be applied to semi-discretization. Optimal convergence can also be observed for quadratic elements and other high-order elements; see Example 5.3 for numerical evidence.

3. Linear elasticity problems with a traction and a body force

3.1. Linear elasticity problems with a traction

When a traction $g=(g_1,g_2)^T$ is applied on the boundary Γ, the Navier's equations are formulated as

$$\begin{aligned}
&-\nabla\cdot\sigma^k=0 && \text{in } \Omega_k,\\
&\sigma^k\cdot n=g^k && \text{on } \Gamma_k,\\
&u^{k-1}|_{\theta=\theta_k^-}=u^k|_{\theta=\theta_k^+},\\
&\sigma^{k-1}\cdot n_k|_{\theta=\theta_k^-}=\sigma^k\cdot n_k|_{\theta=\theta_k^+},
\end{aligned}\tag{3.1}$$

where $k=1,\ldots,K$, $g^k=g|_{\Gamma_k}$ and

$$n=\frac{1}{\sqrt{\tilde r'^2+\tilde r^2}}\big(\tilde r\cos(\phi)+\tilde r'\sin(\phi),\tilde r\sin(\phi)-\tilde r'\cos(\phi)\big)^T$$

is the outward unit normal to Γ. Assume that g satisfies

$$\int_\Gamma g_1 ds=\int_\Gamma g_2 ds=\int_\Gamma(g_2x-g_1y)ds=0.$$

Then the solution of (3.1) is unique up to a rigid displacement. In order to obtain a unique solution, we need three additional conditions, for example

$$u_1|_{\rho=0,\phi=\theta_{K-1}} = u_1|_{\rho=0,\phi=\theta_K} = u_2|_{\rho=0,\phi=\theta_K} = 0. \tag{3.2}$$

Inspired by the discussion on the Dirichlet problem, we assume that the numerical solution of (3.1) takes the form of

$$u^h(\rho,\phi) = N(\phi)^T S(\rho) S(0)^{-1} F, \tag{3.3}$$

where F is unknown in this case. We now need to determine F by the Neumann boundary condition, from which we know that

$$\sum_{k=1}^{K} \int_{\Gamma_k} (\sigma^k \cdot n) \cdot v^h ds = \sum_{k=1}^{K} \int_{\Gamma_k} g^k \cdot v^h ds, \quad \forall v^h \in W^h. \tag{3.4}$$

Noting that $ds = \sqrt{\tilde{r}^2 + (\tilde{r}')^2} d\phi$ and substituting (3.3) into (3.4), we have

$$HF = G, \tag{3.5}$$

where

$$H = \sum_{k=1}^{K} \int_{\theta_k}^{\theta_{k+1}} \left(N(\phi) \Psi_2^k N(\phi)^T S'(0) S(0)^{-1} + N(\phi) \Psi_1^k N'(\phi)^T \right) d\phi,$$
$$G = \sum_{k=1}^{K} \int_{\theta_k}^{\theta_{k+1}} \sqrt{\tilde{r}(\phi)^2 + \left(\tilde{r}'(\phi)\right)^2} N(\phi) g d\phi.$$

In general, H is not invertible and hence we cannot uniquely determine F from (3.5). By the additional conditions (3.2), we know that

$$f_M = f_{2M} = f_j = 0, \tag{3.6}$$

where f_M, f_{2M}, f_j are the M-th, $2M$-th and j-th entries of F with $\phi_j = \theta_{K-1}$. By combining (3.5) and (3.6), we can uniquely determine F and hence the numerical solution of (3.1).

3.2. Linear elasticity problems with a body force

In the presence of a body force $p = (p_1, p_2)^T$, the elastostatic equations are formulated as

$$\begin{aligned} -\nabla \cdot \sigma^k &= p^k && \text{in } \Omega_k, \\ u^k &= f^k && \text{on } \Gamma_k, \\ u^{k-1}|_{\theta=\theta_k^-} &= u^k|_{\theta=\theta_k^+}, \\ \sigma^{k-1} \cdot n_k|_{\theta=\theta_k^-} &= \sigma^k \cdot n_k|_{\theta=\theta_k^+}, \end{aligned} \tag{3.7}$$

where $k = 1, \ldots, K$ and $p^k = (p_1^k, p_2^k)^T = p|_{\Omega_k}$. Applying the transformation of coordinates (2.1), similarly to (2.7), we have

$$-e^{2\rho}\tilde{r}(\phi)^2 \nabla \cdot \sigma^k = -\big(Q_1^k, Q_2^k\big)^T = e^{2\rho}\tilde{r}(\phi)^2 \big(p_1^k, p_2^k\big)^T.$$

Then the corresponding semi-discrete approximation would lead to the following inhomogeneous second-order ODE system:

$$\begin{aligned} &B_2 U''(\rho) + B_1 U'(\rho) + B_0 U(\rho) = P(\rho), \quad -\infty < \rho < 0, \\ &U|_{\rho=0} = F, \end{aligned} \tag{3.8}$$

where U is bounded when $\rho \to -\infty$ and

$$P(\rho) = -\int_0^{2\pi} e^{2\rho}\tilde{r}^2(\phi) N(\phi) p(\rho, \phi) d\phi.$$

The solution of (3.8) could be written as

$$U(\rho) = U_G(\rho) + U_P(\rho),$$

where U_G is the general solution whose expression is exactly (2.28) and U_P is a particular solution satisfying

$$B_2 U_P''(\rho) + B_1 U_P'(\rho) + B_0 U_P(\rho) = P(\rho).$$

Once U_P is found, we can obtain

$$\alpha = S(0)^{-1}\big(F - U_P(0)\big),$$

and hence

$$u^h(\rho, \phi) = N(\phi)^T \left(S(\rho)S(0)^{-1}\big(F - U_P(0)\big) + U_P(\rho)\right). \tag{3.9}$$

In some cases, it is easy to find U_P. For example, if $p = p(\phi)$ and $\gamma = 2$ is not an eigenvalue of (2.26), then

$$U_P(\rho) = (4B_2 + 2B_1 + B_0)^{-1} P(\rho). \tag{3.10}$$

For more general cases, we can convert (3.8) to the Sturm-Liouville boundary value problem, which we will study in the future.

4. Inverse elasticity problems

In this section, the inverse elasticity problem is considered, where we estimate the Lamé coefficients from a measurement of the displacement. Recall that we are interested in the case of composite materials in a star-shaped domain, where each interface between different materials is a line segment connecting the origin and a point on the boundary. We aim to recover the locations of the interfaces and the values of Lamé coefficients on each subdomain.

4.1. Formulation as a regularized minimization problem

We first formulate the inverse elasticity problem as a regularized minimization problem in a more general setting. Consider

$$\begin{aligned} -\nabla\cdot\sigma &= p \quad && \text{in } \Omega,\\ u &= (0,0)^T && \text{on } \Gamma_1,\\ \sigma\cdot n &= g && \text{on } \Gamma_2, \end{aligned} \tag{4.1}$$

where $\Omega\subset\mathbb{R}^2$ is a star-shaped domain, $\partial\Omega=\Gamma_1\cup\Gamma_2$ with $\Gamma_1\cap\Gamma_2=\varnothing$ and n is the outward unit normal to Γ_2. We denote $\ell=(\mu,\lambda)$ and let $u[\ell]$ be the solution of (4.1) with ℓ as the Lamé coefficients. Since we are interested in the case where there are jump discontinuities in the Lamé coefficients, we assume that for some constants $C_1, C_2>0$

$$\begin{aligned} \ell\in\Lambda := \big\{\ell=(\mu,\lambda)\in L^\infty(\Omega)\times L^\infty(\Omega)\,|\,\\ C_1\le\mu,\lambda\le C_2, \mathrm{TV}(\mu)<\infty, \mathrm{TV}(\lambda)<\infty\big\}, \end{aligned} \tag{4.2}$$

where for any $v\in L^1(\Omega)$, $\mathrm{TV}(v)$ is the total variation of v [47], which is defined as

$$\mathrm{TV}(v)=\sup\left\{\iint_\Omega \big(v(\nabla\cdot w)\big)dxdy \,\Big|\, w\in\big(C_0^1(\Omega)\big)^2, |w(x)|\le 1,\ \forall x\in\Omega\right\} \tag{4.3}$$

with $|\cdot|$ as the Euclidean norm of a vector. In the inverse elasticity problem with full-field data, we are given a noisy measurement $z(x,y)$ of $u[\ell^\star](x,y)$ with $\ell^\star=(\mu^\star,\lambda^\star)\in\Lambda$ and $(x,y)\in\Omega$, and we aim to reconstruct $\ell^\star$ from the measurement z.

For the reconstruction of $\ell^\star$, we minimize an energy functional with total variation regularization [29], since with total variation we can effectively recover Lamé coefficients with jump discontinuities [47]. We consider

$$\begin{aligned} \min_{\ell\in\Lambda} J(\ell) := \frac{1}{2}\iint_\Omega \big(2\mu|\varepsilon(u[\ell]-z)|^2+\lambda|\nabla\cdot(u[\ell]-z)|^2\big)\,dx\,dy\\ +\eta\big(\mathrm{TV}(\mu)+\mathrm{TV}(\lambda)\big), \end{aligned} \tag{4.4}$$

where $\eta>0$ is the regularization parameter, and we set

$$J_0(\ell)=\frac{1}{2}\iint_\Omega \big(2\mu|\varepsilon(u[\ell]-z)|^2+\lambda|\nabla\cdot(u[\ell]-z)|^2\big)\,dx\,dy.$$

For the existence of the solution of (4.4), we have the following theorem, which is a special case of [16, Theorem 4.3].

Theorem 4.1. *The minimization problem* (4.4) *admits a solution* $\ell^0\in\Lambda$.

4.2. Numerical procedures for the regularized minimization problem

We still consider the problem in the curvilinear coordinate (2.1). In the case of composite materials, both of the true Lamé coefficients $\mu^\star$ and $\lambda^\star$ are constants in the ρ-direction for fixed ϕ and are piecewise constant functions in the ϕ-direction for fixed ρ. Hence, we let

$$0 = \varphi_0 < \varphi_1 < \cdots < \varphi_m = 2\pi$$

and define

$$\Lambda_h = \Bigg\{ \ell_h(\rho,\phi) = (\mu_h, \lambda_h) \in \Lambda \,\Bigg|\, \begin{matrix} \mu_h, \lambda_h \text{ are constants almost everywhere,} \\ \text{on } (-\infty, 0] \times [\varphi_i, \varphi_{i+1}) \text{ for } i = 0, 1, \ldots, m-1. \end{matrix} \Bigg\}, \tag{4.5}$$

where $h = \max_{0\le i<m} |\varphi_{i+1} - \varphi_i|$. We discretize (4.4) by the following discrete minimization problem:

$$\begin{aligned} \min_{\ell_h \in \Lambda_h} J(\ell_h) = \frac{1}{2} \sum_{k=1}^{m} \int_{-\infty}^{0} \int_{\varphi_{k-1}}^{\varphi_k} \left(2\mu_h |\varepsilon(u[\ell_h] - z)|^2 + \lambda_h |\nabla \cdot (u[\ell_h] - z)|^2 \right) e^{2\rho} \tilde{r}(\phi)^2 d\phi \, d\rho \\ + \eta\big(\mathrm{TV}(\mu_h) + \mathrm{TV}(\lambda_h)\big). \end{aligned} \tag{4.6}$$

The minimizer $\ell_h^\star \in \Lambda_h$ obtained by solving (4.6) is the numerical approximation of the solution of (4.4). For the existence of the solution of (4.6), we have the following theorem, which can be proved with Theorem 4.1 and the fact that Λ_h is a closed subset of Λ with respect to the L^1 metric.

Theorem 4.2. *The minimizing problem* (4.6) *admits a solution* $\ell_h^0 \in \Lambda_h$.

We solve the minimization problem (4.6) by the Adam algorithm [33]. Suppose that

$$\begin{aligned} \mu_h(\rho,\phi) &= \mathbb{1}_{(-\infty,0]}(\rho) \sum_{j=1}^{m} \mu_j \mathbb{1}_{[\varphi_{j-1},\varphi_j)}(\phi), \\ \lambda_h(\rho,\phi) &= \mathbb{1}_{(-\infty,0]}(\rho) \sum_{j=1}^{m} \lambda_j \mathbb{1}_{[\varphi_{j-1},\varphi_j)}(\phi). \end{aligned} \tag{4.7}$$

Then we have

$$\begin{aligned} \mathrm{TV}(\mu_h) &= \sum_{j=1}^{m} \tilde{r}(\varphi_j) |\mu_{j+1} - \mu_j|, \\ \mathrm{TV}(\lambda_h) &= \sum_{j=1}^{m} \tilde{r}(\varphi_j) |\lambda_{j+1} - \lambda_j|, \end{aligned}$$

where $\mu_{m+1} = \mu_1, \lambda_{m+1} = \lambda_1$. The Adam algorithm requires the computation of the gradient of J and hence the gradients of TV(μ_h) and TV(λ_h). In order to avoid the non-differentiability of the absolute value $|\cdot|$ at the origin, we approximate TV(μ_h) and TV(λ_h) by

$$\begin{aligned}\mathrm{TV}_\nu(\mu_h) &= \sum_{j=1}^{m} \tilde{r}(\varphi_j)\sqrt{|\mu_{j+1}-\mu_j|^2+\nu^2},\\ \mathrm{TV}_\nu(\lambda_h) &= \sum_{j=1}^{m} \tilde{r}(\varphi_j)\sqrt{|\lambda_{j+1}-\lambda_j|^2+\nu^2},\end{aligned}$$

respectively, where $0 < \nu \ll 1$ is a small parameter. Instead of minimizing J, we obtain $\ell_h^\star \in \Lambda_h$ by minimizing the following regularized energy functional over $\ell_h \in \Lambda_h$:

$$\begin{aligned}J_\nu(\ell_h) := \frac{1}{2}\sum_{k=1}^{m}\int_{-\infty}^{0}\int_{\varphi_{k-1}}^{\varphi_k} \big(2\mu_h|\varepsilon(u[\ell_h]-z)|^2 + \lambda_h|\nabla\cdot(u[\ell_h]-z)|^2\big)\, e^{2\rho}\tilde{r}(\phi)^2 d\phi\, d\rho\\ + \eta\big(\mathrm{TV}_\nu(\mu_h)+\mathrm{TV}_\nu(\lambda_h)\big).\end{aligned} \tag{4.8}$$

To compute the gradient of J_ν, we have for $j = 1, \ldots, m$

$$\begin{aligned}\frac{\partial \mathrm{TV}_\nu(\mu_h)}{\partial \mu_j} &= \tilde{r}(\varphi_{j-1})\frac{\mu_j-\mu_{j-1}}{\sqrt{|\mu_j-\mu_{j-1}|^2+\nu^2}} + \tilde{r}(\varphi_j)\frac{\mu_j-\mu_{j+1}}{\sqrt{|\mu_j-\mu_{j+1}|^2+\nu^2}},\\ \frac{\partial \mathrm{TV}_\nu(\lambda_h)}{\partial \lambda_j} &= \tilde{r}(\varphi_{j-1})\frac{\lambda_j-\lambda_{j-1}}{\sqrt{|\lambda_j-\lambda_{j-1}|^2+\nu^2}} + \tilde{r}(\varphi_j)\frac{\lambda_j-\lambda_{j+1}}{\sqrt{|\lambda_j-\lambda_{j+1}|^2+\nu^2}},\end{aligned}$$

where $\mu_0 = \mu_m, \lambda_0 = \lambda_m$, $\mu_{m+1} = \mu_1, \lambda_{m+1} = \lambda_1$. Moreover, by the chain rule, we have

$$\begin{aligned}\frac{\partial J_0}{\partial \mu_j} &= \int_{-\infty}^{0}\int_0^{2\pi}\frac{\partial J_0}{\partial \mu_h}\frac{\partial \mu_h}{\partial \mu_j}e^{2\rho}\tilde{r}(\phi)^2 d\phi\, d\rho = \int_{-\infty}^{0}\int_{\varphi_{j-1}}^{\varphi_j}\frac{\partial J_0}{\partial \mu_h}e^{2\rho}\tilde{r}(\phi)^2 d\phi\, d\rho,\\ \frac{\partial J_0}{\partial \lambda_j} &= \int_{-\infty}^{0}\int_0^{2\pi}\frac{\partial J_0}{\partial \lambda_h}\frac{\partial \lambda_h}{\partial \lambda_j}e^{2\rho}\tilde{r}(\phi)^2 d\phi\, d\rho = \int_{-\infty}^{0}\int_{\varphi_{j-1}}^{\varphi_j}\frac{\partial J_0}{\partial \lambda_h}e^{2\rho}\tilde{r}(\phi)^2 d\phi\, d\rho,\end{aligned}$$

and we know from [16] that

$$\begin{aligned}\frac{\partial J_0}{\partial \mu_h} &= -\varepsilon\big(u[\ell_h]+z\big)\cdot\varepsilon\big(u[\ell_h]-z\big),\\ \frac{\partial J_0}{\partial \lambda_h} &= -\frac{1}{2}\big(\nabla\cdot(u[\ell_h]+z)\big)\cdot\big(\nabla\cdot(u[\ell_h]-z)\big).\end{aligned}$$

Hence, for $j = 1, \ldots, m$

$$\frac{\partial J_\nu}{\partial \mu_j} = \frac{\partial J_0}{\partial \mu_j} + \eta\frac{\partial \mathrm{TV}_\nu(\mu_h)}{\partial \mu_j}, \quad \frac{\partial J_\nu}{\partial \lambda_j} = \frac{\partial J_0}{\partial \lambda_j} + \eta\frac{\partial \mathrm{TV}_\nu(\lambda_h)}{\partial \lambda_j}. \tag{4.9}$$

As we can see from the above discussion, the evaluation of $u[\ell_h]$ is needed to obtain the value of J_ν and the gradient of J_ν. Since $\ell_h \in \Lambda_h$, the forward problem is an interface

problem. Hence, the solution $u[\ell_h]$ may admit stress singularities at the intersection point of the interfaces. Moreover, the star-shaped domain is generally irregular. To cope with these two issues, we will apply the direct method of lines as the forward solver.

Denoting

$$\mathscr{L} = (\mu_1, \cdots, \mu_m, \lambda_1, \cdots, \lambda_m)^T,$$
$$\mathcal{G} = \left(\frac{\partial J_\nu}{\partial \mu_1}, \cdots, \frac{\partial J_\nu}{\partial \mu_m}, \frac{\partial J_\nu}{\partial \lambda_1}, \cdots, \frac{\partial J_\nu}{\partial \lambda_m}\right)^T,$$

we let $\mathscr{L}^k$ be the value of $\mathscr{L}$ at the k-th step, $\ell_h^k = (\mu_h^k, \lambda_h^k)$ be the Lamé coefficients (4.7) associated with $\mathscr{L}^k$, and $\mathcal{G}^k$ be the value of $\mathcal{G}$ evaluated at ℓ_h^k. We can summarize the Adam algorithm with the direct method of lines for the inverse elasticity problem in Algorithm 4.1.

Algorithm 4.1

Input: measurement z, initial value $\mathscr{L}^0$, parameters of J_ν including ν and η, and parameters of the algorithm including exponential decay rates $\hat{\beta}_1, \hat{\beta}_2$, a constant $\hat{\epsilon}$, learning rates at each step τ_k and tolerance tol.
Initialize $k = 0$ and $\mathcal{M}^0 = \mathcal{V}^0 = (0, \ldots, 0)^T \in \mathbb{R}^{2m}$.
Compute $u[\ell_h^0]$ using the direct method of lines and compute J_ν^0 via (4.8).
do
    Compute $\mathcal{G}^k$ via (4.9).
    $\mathcal{M}^{k+1} = \hat{\beta}_1 \mathcal{M}^k + (1 - \hat{\beta}_1)\mathcal{G}^k$.
    $\mathcal{V}^{k+1} = \hat{\beta}_2 \mathcal{V}^k + (1 - \hat{\beta}_2)\mathcal{G}^k \odot \mathcal{G}^k$, where $\mathcal{G}^k \odot \mathcal{G}^k$ returns the elementwise square of $\mathcal{G}^k$.
    $\widetilde{\mathcal{M}}^{k+1} = \mathcal{M}^{k+1}/(1 - (\hat{\beta}_1)^{k+1})$.
    $\widetilde{\mathcal{V}}^{k+1} = \mathcal{V}^{k+1}/(1 - (\hat{\beta}_2)^{k+1})$.
    $\mathscr{L}^{k+1} = \mathscr{L}^k - \tau_k \widetilde{\mathcal{M}}^{k+1}/(\sqrt{\widetilde{\mathcal{V}}^{k+1}} + \hat{\epsilon})$.
    Set $k := k + 1$.
    Compute $u[\ell_h^k]$ using the direct method of lines and compute J_ν^k via (4.8).
while $|J_\nu^k - J_\nu^{k-1}|/|J_\nu^{k-1}| > tol$.
Output: $\mathscr{L}^{\tilde{k}}$ for some integer $\tilde{k} > 0$.

5. Numerical examples

5.1. The forward problems

In Examples 5.1 and 5.2, we obtain the numerical solutions and the eigenvalues of the semi-discrete approximation using the linear elements for semi-discretization, while the reference solutions and reference eigenvalues are obtained by using the quadratic elements with fine meshes for semi-discretization. We also compare the effectiveness of

linear elements and quadratic elements for semi-discretization in Example 5.3, where an exact solution is given. We define the L^2 norm $\|\cdot\|_2$ and the energy norm $\|\cdot\|_\star$ by

$$\|v\|_2 = \left(\iint_\Omega \left(|v_1|^2 + |v_2|^2\right) dxdy\right)^{\frac{1}{2}},$$
$$\|v\|_\star = \left(\iint_\Omega \left(2\mu|\varepsilon(v)|^2 + \lambda|\nabla\cdot v|^2\right) dxdy\right)^{\frac{1}{2}},$$

where

$$v = (v_1, v_2)^T \in H^1(\Omega) \times H^1(\Omega).$$

It is easy to see that $\|v\|_\star \leq \|v\|_*$ for any $v \in H^1(\Omega) \times H^1(\Omega)$, where $\|\cdot\|_*$ is defined in Theorem 2.1. We shall consider the L^2 relative error $\|u - u^h\|_2/\|u\|_2$ and the energy relative error $\|u - u^h\|_\star/\|u\|_\star$, where $u = (u_1, u_2)^T$ is the reference/exact solution and $u^h = (u_1^h, u_2^h)^T$ is our numerical solution.

Example 5.1. Let

$$\tilde{r}(\phi) = \sqrt{2 + \cos(4\phi)},$$
$$\Omega = \big\{(r,\phi)\,|\,0 \leq r < \tilde{r}(\phi),\ 0 \leq \phi < 2\pi\big\},$$
$$\Omega_k = \big\{(r,\phi)\,|\,0 < r < \tilde{r}(\phi),\ \theta_k < \phi < \theta_{k+1}\big\},$$

where $k = 1, \ldots, 4$ and $\theta_1 = 0, \theta_2 = \pi/2, \theta_3 = \pi, \theta_4 = 3\pi/2, \theta_5 = 2\pi$ (See Fig. 3).

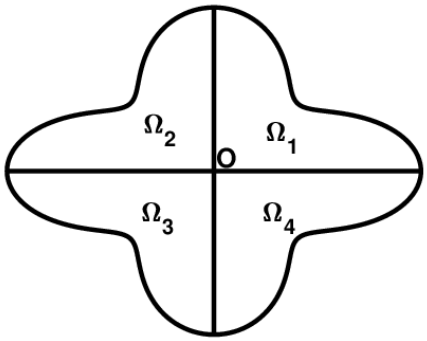

Figure 3: Domain Ω in Example 5.1.

Consider

$$\begin{aligned}
&-\nabla\cdot\sigma^k = p && \text{in } \Omega_k, && k = 1, \ldots, 4,\\
&u = f && \text{on } \Gamma = \partial\Omega, &&\\
&u^{k-1}|_{\theta=\theta_k^-} = u^k|_{\theta=\theta_k^+}, && && k = 1, \ldots, 4,\\
&\sigma^{k-1}\cdot n_k|_{\theta=\theta_k^-} = \sigma^k\cdot n_k|_{\theta=\theta_i=k^+}, && && k = 1, \ldots, 4,
\end{aligned} \tag{5.1}$$

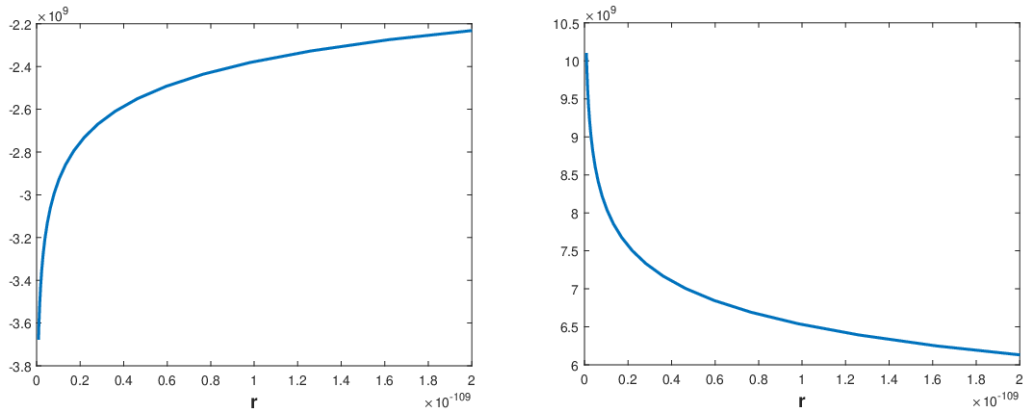

(a) $\partial u_1/\partial r$ (b) $\partial u_2/\partial r$

Figure 4: $\partial u/\partial r(r, \phi_0)$ with $\phi_0 = 3\pi/4$ in Example 5.1.

where

$$(\mu_1, \lambda_1) = \left(\frac{1}{10}, 1\right), \quad (\mu_2, \lambda_2) = \left(\frac{1}{5}, \frac{6}{5}\right), \quad p = (1, 1)^T,$$
$$(\mu_3, \lambda_3) = \left(\frac{3}{10}, \frac{7}{5}\right), \quad (\mu_4, \lambda_4) = \left(\frac{2}{5}, \frac{8}{5}\right), \quad f = (x, y)^T.$$

We show $\partial u/\partial r(r, \phi_0)$ with $\phi_0 = 3\pi/4$ in Fig. 4. We can see that as $r \to 0$, $\partial u_1/\partial r$ and $\partial u_2/\partial r$ approach $-\infty$ and ∞, respectively, which indicates that the stress singularities occur at the origin.

Let M be a positive integer and the partition of $[0, 2\pi]$ be given by

$$0 = \phi_1 < \phi_2 < \cdots < \phi_{M+1} = 2\pi$$

with $h = 2\pi/M$ and $\phi_j = (j-1)h$ for $j = 1, 2, \ldots, M+1$. Errors of the first nonzero eigenvalue γ_3^h of the semi-discrete approximation are given in Table 1 for different M, with the reference eigenvalue $\gamma_3 = 0.9084878530$. We know from Table 1 that the convergence order of γ_3^h is 2, which shows that the eigenvalues of the semi-discrete

Table 1: Errors of γ_3^h in Example 5.1, with $\gamma_3 = 0.9084878530$.

M	$\lvert\gamma_3^h - \gamma_3\rvert$	Convergence order
8	2.316e-1	
16	1.472e-2	0.653
32	4.250e-2	1.792
64	7.567e-3	2.490
128	1.869e-3	2.018

Table 2: L^2 and energy relative errors of u^h in Example 5.1.

M	$\|u-u^h\|_2/\|u\|_2$	Convergence order	$\|u-u^h\|_\star/\|u\|_\star$	Convergence order
8	1.777e-1		2.001e-1	
16	9.688e-2	0.875	1.176e-1	0.767
32	3.989e-2	1.280	6.815e-2	0.787
64	1.079e-2	1.886	3.638e-2	0.905
128	2.759e-3	1.968	1.867e-2	0.963

approximation converge quickly to the true eigenvalues of the elliptic operator and hence our method can capture the singularities naturally. The L^2 and energy relative errors of our numerical solutions are shown in Table 2. We can see that the convergence order of the L^2 relative error is 2 and the convergence order of the energy relative error is 1, which is consistent with Theorem 2.1.

Example 5.2. Let

$$\begin{aligned}&\tilde{r}(\phi)=\sqrt{2+\cos(3\phi)},\\&\Omega=\big\{(r,\phi)|0\le r<\tilde{r}(\phi),0\le\phi<2\pi\big\},\\&\Omega_k=\big\{(r,\phi)|0<r<\tilde{r}(\phi),\theta_k<\phi<\theta_{k+1}\big\},\end{aligned}$$

where $k=1,2,3$ and $\theta_1=0,\theta_2=\pi/2,\theta_3=5\pi/4,\theta_4=2\pi$ (See Fig. 5).

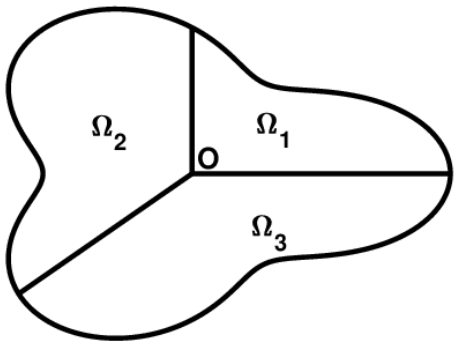

Figure 5: Domain Ω in Example 5.2.

Consider

$$\begin{aligned}&-\nabla\cdot\sigma^k=p && \text{in } \Omega_k, && k=1,2,3,\\&u=f && \text{on } \Gamma=\partial\Omega, &&\\&u^{k-1}|_{\theta=\theta_k^-}=u^k|_{\theta=\theta_k^+}, && && k=1,2,3,\\&\sigma^{k-1}\cdot n_k|_{\theta=\theta_k^-}=\sigma^k\cdot n_k|_{\theta=\theta_k^+}, && && k=1,2,3,\end{aligned}\tag{5.2}$$

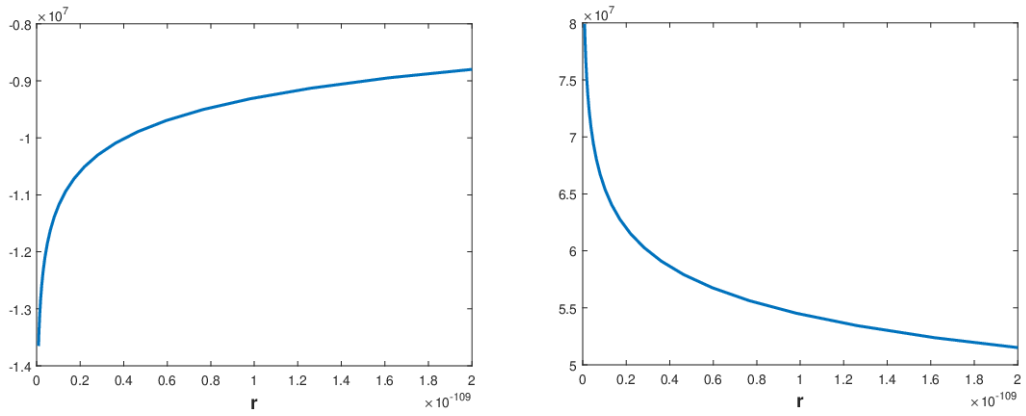

(a) $\partial u_1/\partial r$ (b) $\partial u_2/\partial r$

Figure 6: $\partial u/\partial r(r, \phi_0)$ with $\phi_0 = \pi$ in Example 5.2.

where

$$(\mu_1, \lambda_1) = \left(\frac{2}{7}, 1\right), \quad (\mu_2, \lambda_2) = \left(\frac{3}{7}, \frac{6}{5}\right), \quad (\mu_3, \lambda_3) = \left(\frac{4}{7}, \frac{7}{5}\right),$$
$$p = \left(x\sqrt{x^2+y^2}, y\sqrt{x^2+y^2}\right)^T, \quad f = (1,1)^T.$$

We show $\partial u/\partial r(r, \phi_0)$ with $\phi_0 = \pi$ in Fig. 6 and stress singularities are observed at the origin.

Let M be a positive integer and the partition of $[0, 2\pi]$ be given by

$$0 = \phi_1 < \phi_2 < \cdots < \phi_{M+1} = 2\pi$$

with $h = 2\pi/M$ and $\phi_j = (j-1)h$ for $j = 1, 2, \ldots, M+1$. Errors of the first nonzero eigenvalue γ_3^h of the semi-discrete approximation are given in Table 3 for different M, with the reference eigenvalue $\gamma_3 = 0.9195485286$. The L^2 and energy relative errors of the numerical solution are shown in Table 4. We still observe second-order convergence of γ_3^h, second-order convergence of the L^2 relative error and first-order convergence of the energy relative error.

Table 3: Errors of γ_3^h in Example 5.2, with $\gamma_3 = 0.9195485286$.

M	$\lvert\gamma_3^h - \gamma_3\rvert$	Convergence order
8	1.235e-1	
16	2.845e-2	2.118
32	6.638e-3	2.100
64	1.629e-3	2.027
128	4.053e-4	2.007

Table 4: L^2 and energy relative errors of u^h in Example 5.2.

M	$\|u-u^h\|_2/\|u\|_2$	Convergence order	$\|u-u^h\|_\star/\|u\|_\star$	Convergence order
8	1.940e-3		1.974e-1	
16	8.222e-4	1.176	9.802e-2	1.010
32	1.744e-4	2.237	5.312e-2	0.884
64	4.959e-5	1.814	2.790e-2	0.929
128	1.321e-5	1.908	1.414e-2	0.980

Example 5.3. Let

$$\tilde{r}(\phi)=\begin{cases}-\dfrac{2}{\sin(\phi)}, & -\dfrac{3\pi}{4}\le\phi\le-\dfrac{\pi}{2},\\ 3+\sin(5\phi), & -\dfrac{\pi}{2}<\phi\le\dfrac{\pi}{2},\\ \dfrac{4\sqrt{2}}{\sqrt{\cos(\phi)^4+\sin(\phi)^4+1}}, & \dfrac{\pi}{2}<\phi\le\dfrac{3\pi}{4},\end{cases}$$

and

$$\Omega=\left\{(r,\phi)\,|\,0<r<\tilde{r}(\phi),\,-\frac{3\pi}{4}<\phi<\frac{3\pi}{4}\right\},$$

see Fig. 7.

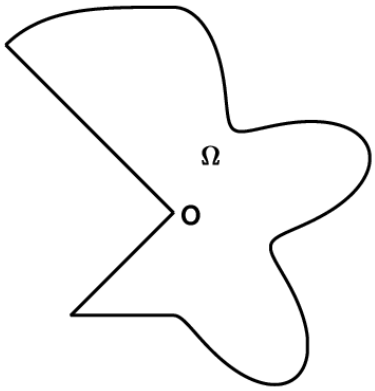

Figure 7: Domain Ω in Example 5.3.

We also let

$$\Gamma_N=\left\{(r,\phi)\,|\,0\le r\le\tilde{r}(\phi),\phi=-\frac{3\pi}{4},\frac{3\pi}{4}\right\},\quad \Gamma_D=\partial\Omega\backslash\Gamma_N.$$

Consider

$$\begin{aligned}-\nabla\cdot\sigma&=(0,0)^T && \text{in } \Omega,\\ u&=f && \text{on } \Gamma_D,\\ \sigma\cdot n&=0 && \text{on } \Gamma_N,\end{aligned}\tag{5.3}$$

where $(\mu, \lambda) = (200, 300)$ and

$$f(r,\phi) = \frac{r^{\gamma_3}}{2\mu}\begin{pmatrix}\big(\kappa - Q(\gamma_3+1)\big)\cos(\gamma_3\phi) - \gamma_3\cos\big((\gamma_3-2)\phi\big)\\ \big(\kappa + Q(\gamma_3+1)\big)\sin(\gamma_3\phi) + \gamma_3\sin\big((\gamma_3-2)\phi\big)\end{pmatrix} \tag{5.4}$$

with γ_3 as the smallest positive root of

$$\sin\left(\gamma_3\frac{3\pi}{2}\right) + \gamma_3\sin\left(\frac{3\pi}{2}\right) = 0, \quad Q = -\frac{\cos\left((\gamma_3-1)3\pi/4\right)}{\cos\left((\gamma_3+1)3\pi/4\right)}, \quad \kappa = 3 - \frac{2\lambda}{\lambda+\mu}.$$

We approximately have $\gamma_3 \approx 0.544483736782464$. Then we know from [18, 45] that $u(r,\phi) = f(r,\phi)$ is the solution of (5.3) and stress singularities occur at the origin.

Let M be a positive integer and the partition of $[-3\pi/4, 3\pi/4]$ be given by

$$-\frac{3\pi}{4} = \phi_1 < \phi_2 < \cdots < \phi_{M+1} = \frac{3\pi}{4}$$

with $h = 3\pi/(2M)$ and $\phi_j = (j-1)h - 3\pi/4$ for $j = 1, 2, \ldots, M+1$. Errors of the first nonzero eigenvalue γ_3^h using linear elements and quadratic elements for semi-discretization are given in Table 5 for different M. We observe that the convergence order of γ_3^h is 2 for linear elements and the convergence order of γ_3^h is 4 for quadratic elements, which again shows that our method can capture the singularities naturally. The relative errors of our numerical solutions using linear elements and quadratic elements are shown in Tables 6 and 7, respectively. We still observe second-order convergence of the L^2 relative error and first-order convergence of the energy relative error using linear elements. For quadratic elements, we observe third-order convergence of the L^2

Table 5: Errors of γ_3^h in Example 5.3 using linear elements and quadratic elements.

	Linear elements		Quadratic elements	
M	$\lvert\gamma_3^h - \gamma_3\rvert$	Convergence order	$\lvert\gamma_3^h - \gamma_3\rvert$	Convergence order
12	8.527e-3		1.428e-3	
24	2.295e-3	1.894	1.029e-4	3.795
48	5.231e-4	2.133	5.966e-6	4.108
96	1.253e-4	2.062	3.734e-7	3.998
192	3.094e-5	2.018	2.340e-8	3.996

Table 6: L^2 and energy relative errors of u^h in Example 5.3 using linear elements.

M	$\lVert u-u^h\rVert_2/\lVert u\rVert_2$	Convergence order	$\lVert u-u^h\rVert_\star/\lVert u\rVert_\star$	Convergence order
12	5.885e-1		2.309e-1	
24	2.119e-1	1.474	1.348e-1	0.777
48	6.048e-2	1.809	6.975e-2	0.950
96	1.567e-2	1.948	3.517e-2	0.988
192	3.954e-3	1.987	1.762e-2	0.997

Table 7: L^2 and energy relative errors of u^h in Example 5.3 using quadratic elements.

M	$\|u-u^h\|_2/\|u\|_2$	Convergence order	$\|u-u^h\|_\star/\|u\|_\star$	Convergence order
12	6.892e-2		7.467e-2	
24	4.359e-3	3.983	1.883e-2	1.988
48	2.782e-4	3.970	4.708e-3	2.000
96	1.871e-5	3.895	1.179e-3	1.998
192	1.671e-6	3.485	2.949e-4	1.999

relative error and second-order convergence of the energy relative error. Hence, optimal convergence is observed for both linear and quadratic elements in the presence of stress singularities, and our method is effective for the linear elasticity problem with both linear and quadratic elements for semi-discretization. In general, faster convergence can be obtained by using higher-order elements for semi-discretization.

In Examples 5.1-5.3, we observe fast convergence of the eigenvalues of the semi-discrete approximation to the true eigenvalue of the elliptic operator, and thus our method can capture the singularities naturally. Moreover, optimal convergence is observed for both linear elements and quadratic elements in the presence of stress singularities. Therefore, our method is effective and accurate for the linear elasticity problem of composite materials in the star-shaped domain.

5.2. The inverse elasticity problems

We use Algorithm 4.1 to minimize (4.8) over $\ell_h \in \Lambda_h$, with $\eta = 10^{-7}, \nu = 10^{-7}, \hat{\beta}_1 = 0.9, \hat{\beta}_2 = 0.999, \hat{\epsilon} = 10^{-7}, tol = 5 \times 10^{-6}$ and a decaying τ_k. We discretize the solution space with mesh size $h = \pi/64$, i.e. we parameterize μ_h and λ_h as

$$\mu_h = \mathbb{1}_{(-\infty,0]}(\rho) \sum_{j=1}^{128} \mu_j \mathbb{1}_{[(j-1)h,jh)}(\phi),$$

$$\lambda_h = \mathbb{1}_{(-\infty,0]}(\rho) \sum_{j=1}^{128} \lambda_j \mathbb{1}_{[(j-1)h,jh)}(\phi).$$

We denote the values of μ_j, λ_j at the k-th step by μ_j^k, λ_j^k, $j = 1, \ldots, 128$, respectively. The forward problem in each iteration is computed using the direct method of lines with linear elements for semi-discretization with mesh size $\tilde{h} = \pi/64$. The noiseless measurement $u[\ell^\star]$ is obtained by using the direct method of lines with quadratic elements for semi-discretization with finer meshes. The measurement is taken at discrete locations

$$\Xi = \{(x_j, y_j)\}_{j=1}^{M_1} \subset \Omega.$$

The L^1 errors of the Lamé coefficients are considered, with the L^1 norm denoted by $\|\cdot\|_1$.

Example 5.4. Let

$$\tilde{r}(\phi) = 1 + \cos(\phi)^2, \quad \Omega = \left\{(r,\phi)\,|\,0 \le r < \tilde{r}(\phi),\, 0 \le \phi < 2\pi\right\}$$

with

$$\begin{aligned}
\Omega_1 &= \left\{(r,\phi)\,|\,0 < r < \tilde{r}(\phi),\, \pi < \phi < \frac{7\pi}{4}\right\},\\
\Omega_2 &= \left\{(r,\phi)\,|\,0 < r < \tilde{r}(\phi),\, \frac{7\pi}{4} < \phi \le 2\pi,\, 0 < \phi < \frac{\pi}{4}\right\},\\
\Omega_3 &= \left\{(r,\phi)\,|\,0 < r < \tilde{r}(\phi),\, \frac{\pi}{4} < \phi < \pi\right\},
\end{aligned}$$

see Fig. 8. Consider

$$\begin{aligned}
&-\nabla\cdot\sigma^k = p && \text{in } \Omega_k, \quad k = 1,2,3,\\
&u = f && \text{on } \Gamma,\\
&u^{k-1}|_{\theta=\theta_k^-} = u^k|_{\theta=\theta_k^+}, && k = 1,2,3,\\
&\sigma^{k-1}\cdot n_k|_{\theta=\theta_k^-} = \sigma^k\cdot n_k|_{\theta=\theta_k^+}, && k = 1,2,3,
\end{aligned} \tag{5.5}$$

where

$$\begin{aligned}
&(\mu_1^\star,\lambda_1^\star) = \left(\frac{3}{7},1\right), \quad (\mu_2^\star,\lambda_2^\star) = \left(\frac{6}{7},2\right), \quad (\mu_3^\star,\lambda_3^\star) = \left(\frac{9}{7},3\right),\\
&p = (1,1)^T, \quad f = (1,1)^T.
\end{aligned}$$

Let

$$z|_\Xi = u[\ell^\star]|_\Xi + \delta\xi_U\|u[\ell^\star]\|_\infty$$

be the noisy measurement, where $\|\cdot\|_\infty$ is the L^∞ norm, ξ_U is a vector of i.i.d. uniformly distributed random variables in $[-1,1]$ and $\delta = 0.0001$ is the noise level.

We start from $\mu_1^0 = \cdots = \mu_{128}^0 = 6/7, \lambda_1^0 = \cdots = \lambda_{128}^0 = 2$ and 319 steps of iterations are implemented before the termination condition is satisfied. The evolution of the value of J with respect to the iteration k is shown in Fig. 9. The numerical Lamé

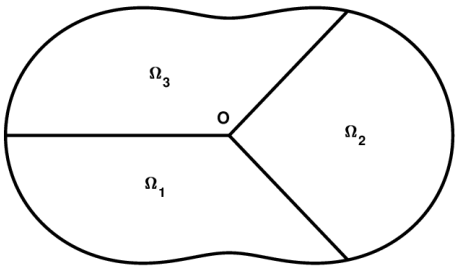

Figure 8: Domain Ω in Example 5.4.

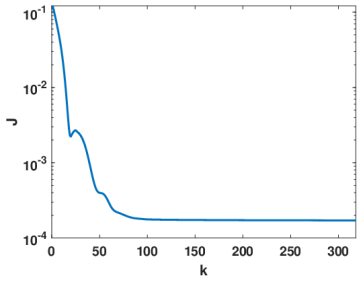

Figure 9: Values of J in Example 5.4.

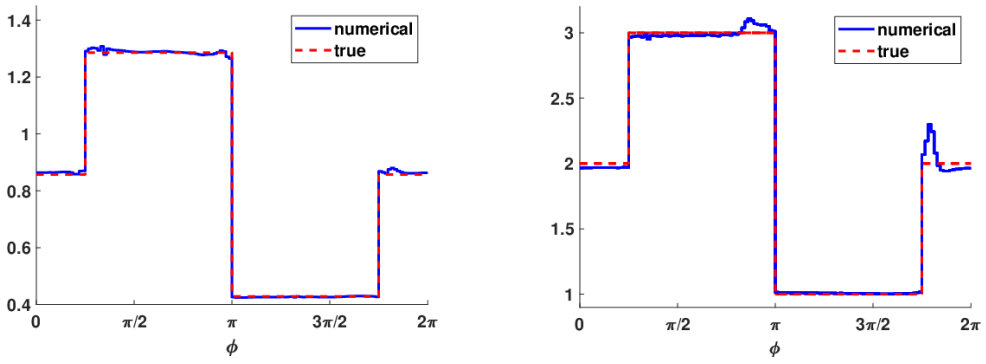

(a) μ (b) λ

Figure 10: Lamé coefficients at the 319-th iteration in the ϕ-direction of Example 5.4.

coefficients μ_h^{319} and λ_h^{319} in the ϕ-direction are plotted as the blue lines in Fig. 10, with the red dotted lines as the true Lamé coefficients. At the 319-th step, the L^1 relative errors of the numerical Lamé coefficients are

$$\frac{\|\mu_h^{319}-\mu^\star\|_1}{\|\mu^\star\|_1}=6.288e-3,\quad \frac{\|\lambda_h^{319}-\lambda^\star\|_1}{\|\lambda^\star\|_1}=1.572e-2,$$

respectively.

Example 5.5. Let

$$\tilde{r}(\phi)=\frac{1}{\sqrt{\cos(\phi)^4+\sin(\phi)^4}},$$
$$\Omega=\left\{(r,\phi)\,|\,0\le r<\tilde{r}(\phi),\,0\le\phi<2\pi\right\}$$

with

$$\Omega_1=\left\{(r,\phi)\,|\,0<r<\tilde{r}(\phi),\,\pi<\phi<\frac{7\pi}{4}\right\},$$
$$\Omega_2=\left\{(r,\phi)\,|\,0<r<\tilde{r}(\phi),\,\frac{7\pi}{4}<\phi\le 2\pi,0<\phi<\frac{\pi}{4}\right\},$$
$$\Omega_3=\left\{(r,\phi)\,|\,0<r<\tilde{r}(\phi),\,\frac{\pi}{4}<\phi<\frac{3\pi}{4}\right\},$$
$$\Omega_4=\left\{(r,\phi)\,|\,0<r<\tilde{r}(\phi),\,\frac{3\pi}{4}<\phi<\pi\right\},$$

see Fig. 11. Consider

$$\begin{aligned}
&-\nabla\cdot\sigma^k=p_1 && \text{in } \Omega_k,\quad k=1,\dots,4,\\
&u=(0,0)^T && \text{on } \Gamma,\\
&u^{k-1}|_{\theta=\theta_k^-}=u^k|_{\theta=\theta_k^+}, && k=1,\dots,4,\\
&\sigma^{k-1}\cdot n_k|_{\theta=\theta_k^-}=\sigma^k\cdot n_k|_{\theta=\theta_k^+}, && k=1,\dots,4,
\end{aligned}\tag{5.6}$$

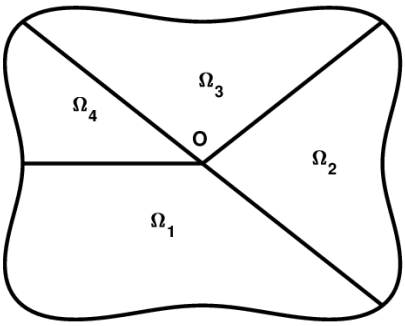

Figure 11: Domain Ω in Example 5.5.

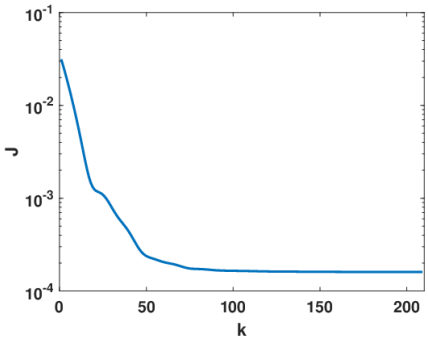

Figure 12: Values of J in Example 5.5.

where

$$(\mu_1^\star, \lambda_1^\star) = \left(\frac{3}{7}, 1\right), \quad (\mu_2^\star, \lambda_2^\star) = \left(\frac{6}{7}, 2\right),$$
$$(\mu_3^\star, \lambda_3^\star) = \left(\frac{9}{7}, 3\right), \quad (\mu_4^\star, \lambda_4^\star) = \left(\frac{6}{7}, 2\right),$$
$$p = \left(\frac{x}{\sqrt{x^2+y^2}} + 1, \frac{y}{\sqrt{x^2+y^2}} + 1\right)^T.$$

Let the noisy measurement

$$z|_\Xi = u[\ell^\star]|_\Xi + \delta\xi_U \|u[\ell^\star]\|_\infty,$$

where ξ_U is a vector of i.i.d. uniformly distributed random variables in $[-1, 1]$ and $\delta = 0.0001$.

We start from $\mu_1^0 = \cdots = \mu_{128}^0 = 6/7, \lambda_1^0 = \cdots = \lambda_{128}^0 = 2$ and 210 steps of iterations are implemented before the termination condition is satisfied. The evolution of the

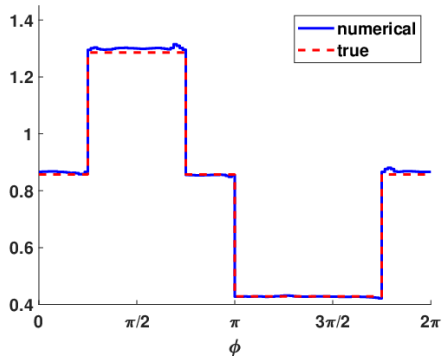

(a) μ

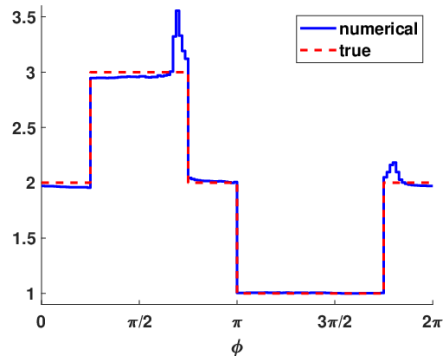

(b) λ

Figure 13: Lamé coefficients at the 210th iteration in the ϕ-direction of Example 5.5.

value of J with respect to the iteration k is shown in Fig. 12. The numerical Lamé coefficients μ_h^{210} and λ_h^{210} in the ϕ-direction are plotted as the blue lines in Fig. 13, with the red dotted lines as the true Lamé coefficients. At the 210-th step, the L^1 relative errors of the numerical Lamé coefficients are

$$\frac{\|\mu_h^{210}-\mu^\star\|_1}{\|\mu^\star\|_1}=8.642e-3,\quad \frac{\|\lambda_h^{210}-\lambda^\star\|_1}{\|\lambda^\star\|_1}=2.027e-2.$$

Example 5.6. We are interested in the influence of the noise in measurement data on the performance of our method. We consider the same settings as in Example 5.4.

Case (i). Let the measurement

$$z|_\Xi = u[\ell^\star]|_\Xi + \delta\xi_U\|u[\ell^\star]\|_\infty,$$

where ξ_U is a vector of i.i.d. uniformly distributed random variables in $[-1,1]$. We choose $\delta=0.0004,0.0007,0.001$. For each δ, we start from $\mu_1^0=\cdots=\mu_{128}^0=6/7, \lambda_1^0=\cdots=\lambda_{128}^0=2$. Before the termination condition is satisfied, $\tilde{k}$ steps of iterations are implemented. The values of $\tilde{k}$ and the L^1 relative errors of the numerical Lamé coefficients at the $\tilde{k}$-th step for each δ are shown in Table 8.

Table 8: Total numbers of iteration $\tilde{k}$ and L^1 relative errors in Case(i) of Example 5.6.

δ	$\tilde{k}$	$\|\mu_h^{\tilde{k}}-\mu^\star\|_1/\|\mu^\star\|_1$	$\|\lambda_h^{\tilde{k}}-\lambda^\star\|_1/\|\lambda^\star\|_1$
0.0004	380	6.437e-3	1.517e-2
0.0007	280	6.709e-3	1.406e-2
0.001	332	6.808e-3	1.186e-2

The numerical Lamé coefficients at the $\tilde{k}$-th step in the ϕ-direction for $\delta=0.0004,0.0007,0.001$ are plotted as the blue lines in Figs. 14-16, respectively, with the red dotted lines as the true Lamé coefficients.

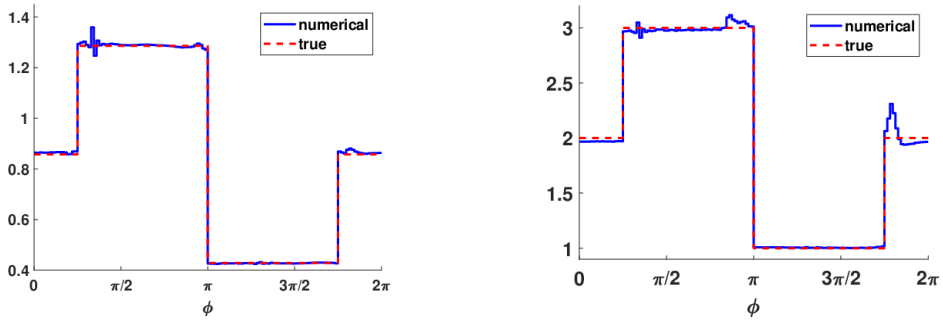

(a) μ (b) λ

Figure 14: Lamé coefficients at the 380-th iteration in the ϕ-direction for $\delta=0.0004$ in Case (i) of Example 5.6.

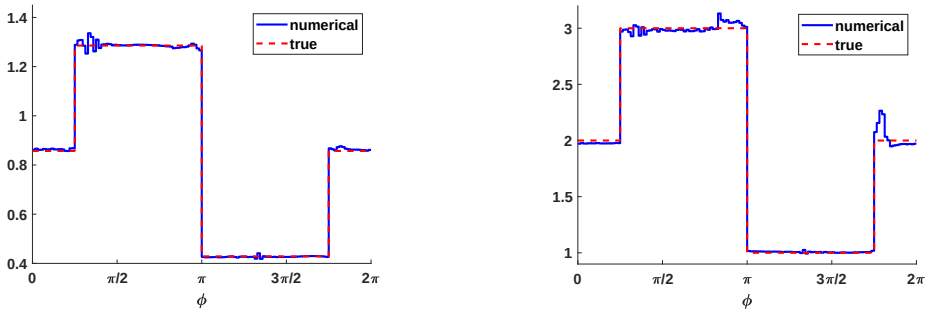

(a) μ (b) λ

Figure 15: Lamé coefficients at the 280-th iteration in the ϕ-direction for $\delta = 0.0007$ in Case (i) of Example 5.6.

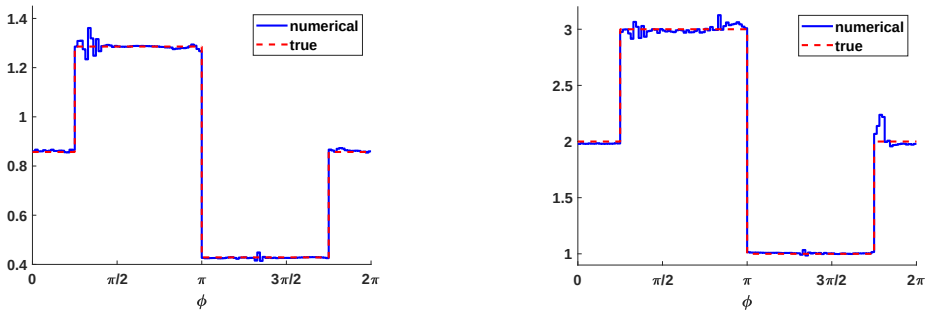

(a) μ (b) λ

Figure 16: Lamé coefficients at the 332-nd iteration in the ϕ-direction for $\delta = 0.001$ in Case (i) of Example 5.6.

Case (ii). Let the measurement

$$z|_\Xi = u[\ell^\star]|_\Xi + \delta\xi_G\|u[\ell^\star]\|_\infty,$$

where ξ_G is a vector of i.i.d. standard Gaussian random variables. We choose $\delta = 0.0004, 0.0007, 0.001$. For each δ, we start from $\mu_1^0 = \cdots = \mu_{128}^0 = 6/7, \lambda_1^0 = \cdots = \lambda_{128}^0 = 2$. Before the termination condition is satisfied, $\tilde{k}$ steps of iterations are implemented. The values of $\tilde{k}$ and the L^1 relative errors of the numerical Lamé coefficient at the $\tilde{k}$-th step for each δ are shown in Table 9.

Table 9: Total numbers of iteration $\tilde{k}$ and L^1 relative errors in Case(ii) of Example 5.6.

δ	$\tilde{k}$	$\|\mu_h^{\tilde{k}} - \mu^\star\|_1/\|\mu^\star\|_1$	$\|\lambda_h^{\tilde{k}} - \lambda^\star\|_1/\|\lambda^\star\|_1$
0.0004	329	8.219e-3	1.745e-2
0.0007	224	1.091e-2	1.975e-2
0.001	140	1.424e-2	3.010e-2

The numerical Lamé coefficients at the $\tilde{k}$-th step in the ϕ-direction for $\delta = 0.0004, 0.0007, 0.001$ are plotted as the blue lines in Figs. 17-19, respectively, with the red dotted lines as the true Lamé coefficients.

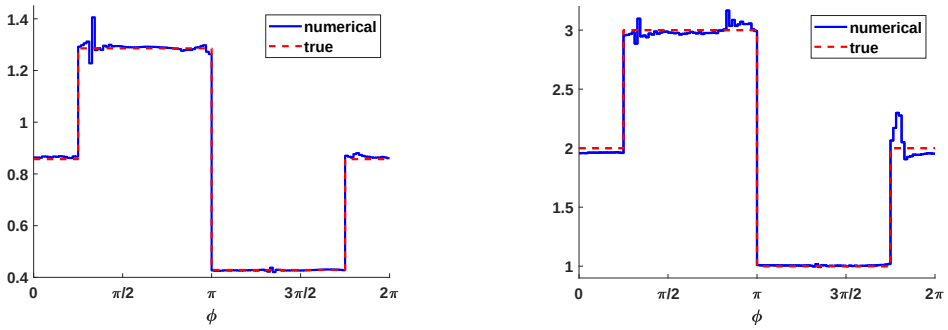

(a) μ (b) λ

Figure 17: Lamé coefficients at the 329-th step in the ϕ-direction for $\delta = 0.0004$ in Case (ii) of Example 5.6.

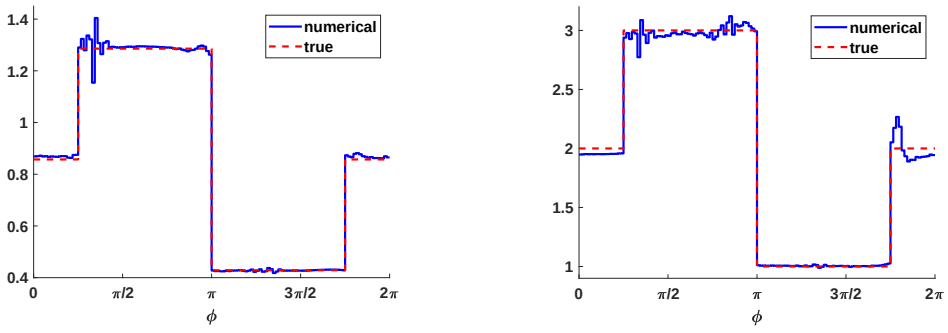

(a) μ (b) λ

Figure 18: Lamé coefficients at the 224-th step in the ϕ-direction for $\delta = 0.0007$ in Case (ii) of Example 5.6.

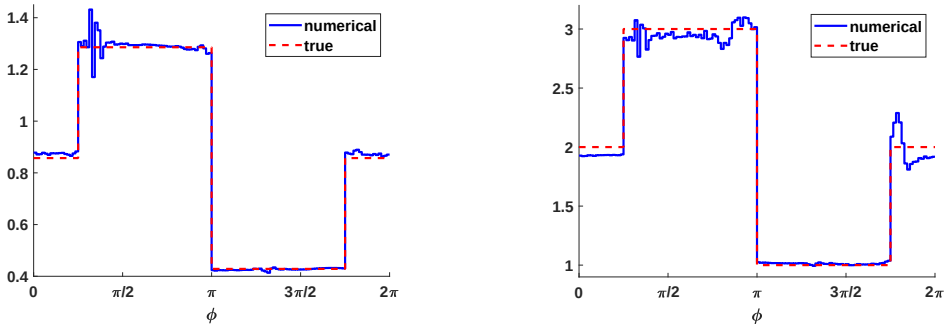

(a) μ (b) λ

Figure 19: Lamé coefficients at the 140-th step in the ϕ-direction for $\delta = 0.001$ in Case (ii) of Example 5.6.

As we can see from Examples 5.4-5.6, our method is effective in recovering both the locations of the interfaces and the values of the Lamé coefficients on each subdomain. In particular, as is shown in Example 5.6, our method is working well for different types of noises and a mild level of noises.

6. Conclusion

In this paper, we consider both the forward and inverse linear elasticity problems of composite materials in star-shaped domains. We generalize the direct method of lines for the linear elasticity problem in star-shaped domains and apply the generalized method to the inverse elasticity problem. We assume that the boundary of the domain can be described by an explicit C^1 parametric curve in the polar coordinate, and to be more precise it can be parameterized as a (piecewise) C^1 function of the angular variable so that we can introduce the curvilinear coordinate. In the curvilinear coordinate, the irregular star-shaped domain is converted to a regular semi-infinite strip and the linear elasticity problem is reduced to a variational-differential problem. By discretizing the variational-differential problem with respect to the angular variable, we obtain a semi-discrete approximation, which is then analytically solved by a direct method. It is numerically found that the eigenvalues of the semi-discrete approximation converge quickly to the true eigenvalues of the elliptic operator, which helps capture the singularities naturally. Moreover, our method has an optimal error estimate and is also able to deal with linear elasticity problems with a traction and a body force. Numerical results demonstrate the effectiveness and accuracy of the direct method of lines for linear elasticity problems in star-shaped domains.

On the other hand, the inverse elasticity problem of composite materials is considered. The Lamé coefficients are approximated by piecewise constant functions and estimated by minimizing an energy functional with total variation regularization using the Adam algorithm. In each iteration, the forward problem is an interface problem in the star-shaped domain. Hence, the direct method of lines is applied as the forward solver to cope with the irregularity of the star-shaped domain and possible singularities in the forward solutions. It is numerically shown that we can successfully recover the locations of the interfaces and the values of Lamé coefficients on each subdomain using our method.

In the future, we will consider numerical methods for the linear elastic problem with singularities in more general domains and for the important case of nearly incompressible linear elasticity.

Acknowledgments

This work was partially supported by the NSFC Projects No. 12025104, 11871298, 81930119.

References

[1] O. A. Babaniyi, A. A. Oberai, and P. E. Barbone, *Direct error in constitutive equation formulation for plane stress inverse elasticity problem*, Comput. Methods Appl. Mech. Engrg. 314 (2017), 3–18.

[2] I. Babuška, *Finite element method for domains with corners*, Computing 6 (1970), 264–273.

[3] I. Babuška, *Solution of problems with interfaces and singularities*, in: *Mathematical aspects of finite elements in partial differential equations*, Academic Press, (1974), 213–277.

[4] I. Babuška, *Singularities Problem in the Finite Element Method*, Tech. Note. BN-835, Institute for Fluid Dynamics and Applied Mathematics, University of Maryland, 1976.

[5] I. Babuška, R. B. Kellogg, and J. Pitkäranta, *Direct and inverse error estimates for finite elements with mesh refinements*, Numer. Math. 33 (1979), 447–471.

[6] P. E. Barbone, C. E. Rivas, I. Harari, U. Albocher, A. A. Oberai, Y. Zhang, *Adjoint-weighted variational formulation for the direct solution of inverse problems of general linear elasticity with full interior data*, Int. J. Numer. Methods Eng. 81 (2010), 1713–1736.

[7] J. H. Bramble, B. E. Hubbard, and M. Zlamal, *Discrete analogues of the Dirichlet problem with isolated singularities*, SIAM J. Numer. Anal. 5 (1968), 1–25.

[8] C. Carstensen, G. Dolzmann, S. A. Funken, and D. Helm, *Locking-free adaptive mixed finite element methods in linear elasticity*, Comput. Methods Appl. Mech. Engrg. 190 (2000), 1701–1718.

[9] J. Chang and J.-Q. Xu, *The singular stress field and stress intensity factors of a crack terminating at a bimaterial interface*, Int. J. Mech. Sci. 49 (2007), 888–897.

[10] Y. K. Cheung and C. P. Jiang, *Application of the finite strip method to plane fracture problems*, Eng. Fract. Mech. 53 (1996), 89–96.

[11] M. M. Doyley, *Model-based elastography: A survey of approaches to the inverse elasticity problem*, Phys. Med. Biol. 57 (2012), R35.

[12] A. H. England, *A crack between dissimilar media*, J. Appl. Mech. 32 (1965), 400–402.

[13] G. J. Fix, S. Gulati, and G. I. Wakoff, *On the use of singular functions with finite element approximations*, J. Comput. Phys. 13 (1973), 209–228.

[14] T.-P. Fries, *A corrected XFEM approximation without problems in blending elements*, Int. J. Numer. Methods Eng. 75 (2008), 503–532.

[15] S. S. Ghorashi, N. Valizadeh, and S. Mohammadi, *Extended isogeometric analysis for simulation of stationary and propagating cracks*, Int. J. Numer. Methods Eng. 89 (2012), 1069–1101.

[16] M. Gockenbach and A. Khan, *An abstract framework for elliptic inverse problems: Part 1. An output least-squares approach*, Math. Mech. Solids 12 (2007), 259–276.

[17] M. Gockenbach and A. Khan, *An abstract framework for elliptic inverse problems: Part 2. An augmented Lagrangian approach*, Math. Mech. Solids 14 (2009), 517–539.

[18] O. A. González-Estrada, S. Natarajan, J. J. Ródenas, H. Nguyen-Xuan, and S. Bordas, *Efficient recovery-based error estimation for the smoothed finite element method for smooth and singular linear elasticity*, Comput. Mech. 52 (2013), 37–52.

[19] M. Grédiac, *The use of full-field measurement methods in composite material characterization: Interest and limitations*, Compos. Part A Appl. Sci. Manuf. 35 (2004), 751–761.

[20] M. Grédiac and F. Hild, *Full-Field Measurements and Identification in Solid Mechanics*, John Wiley & Sons, 2012.

[21] J. F. Greenleaf, M. Fatemi, and M. Insana, *Selected methods for imaging elastic properties of biological tissues*, Annu. Rev. Biomed. Eng. 5 (2003), 57–78.

[22] V. GUPTA, C. A. DUARTE, I. BABUŠKA, AND U. BANERJEE, *A stable and optimally convergent generalized FEM (SGFEM) for linear elastic fracture mechanics*, Comput. Methods Appl. Mech. Engrg. 266 (2013), 23–39.
[23] H. HAN, *The numerical solutions of interface problems by infinite element method*, Numer. Math. 39 (1982), 39–50.
[24] H. HAN AND W. BAO, *An artificial boundary condition for two-dimensional incompressible viscous flows using the method of lines*, Int. J. Numer. Methods Fluids 22 (1996), 483–493.
[25] H. HAN AND W. BAO, *The discrete artificial boundary condition on a polygonal artificial boundary for the exterior problem of Poisson equation by using the direct method of lines*, Comput. Methods Appl. Mech. Engrg. 179 (1999), 345–360.
[26] H. HAN AND Z. HUANG, *The direct method of lines for the numerical solutions of interface problem*, Comput. Methods Appl. Mech. Engrg. 171 (1999), 61–75.
[27] H. HAN AND Z. HUANG, *The discrete method of separation of variables for composite material problems*, Int. J. Fract. 112 (2001), 379–402.
[28] S. HUBMER, E. SHERINA, A. NEUBAUER, AND O. SCHERZER, *Lamé parameter estimation from static displacement field measurements in the framework of nonlinear inverse problems*, SIAM J. Imaging Sci. 11 (2018), 1268–1293.
[29] B. JADAMBA, A. A. KHAN, AND F. RACITI, *On the inverse problem of identifying Lamé coefficients in linear elasticity*, Comput. Math. Appl. 56 (2008), 431–443.
[30] B. JADAMBA, A. A. KHAN, G. RUS, M. SAMA, AND B. WINKLER, *A new convex inversion framework for parameter identification in saddle point problems with an application to the elasticity imaging inverse problem of predicting tumor location*, SIAM J. Appl. Math. 74 (2014), 1486–1510.
[31] R. B. KELLOGG, *Singularities in interface problems*, in: *Numerical Solution of Partial Differential Equations-II*, Academic Press, (1971), 351–400.
[32] R. B. KELLOGG, *On the Poisson equation with intersecting interfaces*, Appl. Anal. 4 (1975), 101–129.
[33] D. P. KINGMA AND J. L. BA, *Adam: A Method for Stochastic Gradient Descent*, in: *ICLR: International Conference on Learning Representations*, (2015).
[34] Z. LI AND R. MATHON, *Error and stability analysis of boundary methods for elliptic problems with interfaces*, Math. Comp. 54 (1990), 41–61.
[35] K. Y. LIN AND J. W. MAR, *Finite element analysis of stress intensity factors for cracks at a bi-material interface*, Int. J. Fract. 12 (1976), 521–531.
[36] P. P. L. MATOS, R. M. MCMEEKING, P. G. CHARALAMBIDES, AND M. D. DRORY, *A method for calculating stress intensities in bimaterial fracture*, Int. J. Fract. 40 (1989), 235–254.
[37] H.-S. OH AND I. BABUŠKA, *The method of auxiliary mapping for the finite element solutions of elasticity problems containing singularities*, J. Comput. Phys. 121 (1995), 193–212.
[38] P. PAPADAKIS AND I. BABUŠKA, *A numerical procedure for the determination of certain quantities related to the stress intensity factors in two-dimensional elasticity*, Comput. Methods Appl. Mech. Engrg. 122 (1995), 69–92.
[39] K. J. PARKER, M. M. DOYLEY, AND D. J. RUBENS, *Imaging the elastic properties of tissue: The 20 year perspective*, Phys. Med. Biol. 56 (2010), R1.
[40] S. T. RAVEENDRA AND P. K. BANERJEE, *Computation of stress intensity factors for interfacial cracks*, Eng. Fract. Mech. 40 (1991), 89–103.
[41] J. R. RICE, *Elastic fracture mechanics concepts for interfacial cracks*, J. Appl. Mech. 55 (1988), 98–103.
[42] J. R. RICE AND G. C. SIH, *Plane problems of cracks in dissimilar media*, J. Appl. Mech. 32 (1965), 418–423.

[43] M. ROSSI AND F. PIERRON, *On the use of simulated experiments in designing tests for material characterization from full-field measurements*, Int. J. Solids Struct. 49 (2012), 420–435.
[44] W. E. SCHIESSER, *The Numerical Method of Lines: Integration of Partial Differential Equations*, Elsevier, 2012.
[45] B. A. SZABÓ AND I. BABUŠKA, *Finite Element Analysis*, Wiley, 1991.
[46] F. TISSEUR AND K. MEERBERGEN, *The quadratic eigenvalue problem*, SIAM Rev. 43 (2001), 235–286.
[47] C. R. VOGEL, *Computational Methods for Inverse Problems*, SIAM, 2002.
[48] T. P. WIHLER, *Locking-free adaptive discontinuous Galerkin FEM for linear elasticity problems*, Math. Comp. 75 (2006), 1087–1102.
[49] M. WILLIAMS, *The stresses around a fault or crack in dissimilar media*, Bull. Seismol. Soc. Am. 49 (1959), 199–204.
[50] Z. WU, Z. HUANG, W.-C. WANG, AND Y. YANG, *The direct method of lines for elliptic problems in star-shaped domains*, J. Comput. Appl. Math. 327 (2018), 350–361.
[51] L. S. XANTHIS AND C. SCHWAB, *The method of arbitrary lines*, C.R. Acad. Sci., Série 1, Mathématique 312 (1991), 181–187.
[52] Y. Y. YANG AND D. MUNZ, *Stress singularities in a dissimilar materials joint with edge tractions under mechanical and thermal loadings*, Int. J. Solids Struct. 34 (1997), 1199–1216.